An integrated real-time optimization, control, and estimation scheme for post-combustion CO_2 capture

Gabriel D. Patrón[a], Luis Ricardez-Sandoval[a]*

[a]Department of Chemical Engineering, University of Waterloo, Waterloo, ON, Canada N2L 3G1

Abstract

This study presents a novel operational scheme for post-combustion CO_2 capture (PCC) plants downstream from fuel-fired power plants. The approach is comprised of real-time optimization (RTO), nonlinear model predictive control (NMPC), and moving horizon estimation (MHE) layers. These layers are integrated to operate the system economically via a new economic function that accounts for the most significant economic aspects of PCC, including the carbon economy, energy, chemical, and utility costs. The proposed approach was employed on the case study of an MEA-based PCC absorber section, which uses a mechanistic process model to provide an accurate representation of the system. The NMPC layer is novel in its ability to enable flexible control of the plant by manipulating fresh material streams to impact CO_2 capture and the MHE layer is the first to provide accurate system estimates to the controller with realistically accessible measurements. The proposed scheme was subjected to a cofiring scenario, whereby the switching between two fuels is reflected in the flue gas composition. In this scenario, a ~19% steady-state cost improvement is observed with respect to the pre-disturbance cost. Moreover, the MHE was shown to cause an acceptable ~0.5% of performance loss in the process economics through its effect on the NMPC. The scheme was also subjected to a ±20% diurnal variation in power plant load through steps in the flue gas flowrate and was found to provide consistent steady-state economic improvements (from ~12% cost improvement to ~17% loss abatement) for each of the disturbances observed. Furthermore, a price variation scenario highlighted the operational dependence of the system upon changes in economic incentives via the prices. When compared to a 'no RTO' case, the scheme was found to yield economic improvement ranging from ~3% to ~14% depending on the pricing. All scenarios in the case study displayed steady-state cost savings that exceeded the energy penalty imposed on the power plant by the PCC plant. This suggests the proposed scheme is an effective framework for the economic operation of a general class of PCC plants (i.e., with different solvents, process designs and control schemes, etc.) and can help enable the viability of PCC for the continued use of fuel-firing.

Keywords: Post-combustion CO_2 capture; Real-time optimization; Model predictive control; Moving horizon estimation

*Corresponding author: e-mail: laricard@uwaterloo.ca, phone: (+1) 519 888 4567 x38667, fax, (+1) 519 888 4347

1. Introduction

Despite the worldwide energy supply transitioning to renewables, combustion-based energy generation remains necessary to meet surging demands. This is particularly essential for developing economies that must provide inexpensive and reliable energy to their populations. In 2019, combustible fuels accounted for ~79% of the world's energy supply [1], comprising mainly oil, natural gas, and coal. These fuels produce large amounts of carbon dioxide (CO_2), and their continued ubiquity has raised concern by environmental regulatory bodies because of the potency of CO_2 as a greenhouse gas contributing to global warming. To mitigate this effect, the use of carbon capture and storage (CCS) to sequester CO_2 from industrial sources, often power plants, is being widely investigated. Once the CO_2 is captured, it can either be utilized in the manufacturing of new products, or it can be deposited in repositories.

Various methods to achieve CCS have been proposed and implemented, including pre-combustion removal [2], whereby the fuel and CO_2 are gasified and separated prior to combustion; post-combustion removal [3], whereby flue gases are scrubbed after combustion; chemical looping combustion [4,5], which uses an oxygen carrier in the combustion process to generate a CO_2-rich product; and oxy-fuel combustion [6], which uses pure oxygen instead of air to produce a CO_2-rich product. From these methods, post-combustion capture (PCC) is the most mature technology and an attractive option as it allows for easy implementation and retrofitting within existing power plants. PCC can be achieved through a wide array of processes; however, amine solvent absorption has emerged as the forerunner because of the efficacy and availability of the required solvents. Monoethanolamine (MEA) is a common choice of solvent for PCC plants, and its use has been widely explored in academia and industry, prompting the construction of both pilot [7,8] and industrial-scale [9,10] plants. Despite the construction of these few plants, widespread uptake of PCC systems has been slow. The main factor hindering adoption of this technology remains the economic detriment it poses to the fuel-fired power plants to which it is connected; as the PCC process is expensive, it reduces the profit of the power plant. To this end, techno-economic analysis [11,12] and economic operation of the PCC process [13–15] have been studied. These economical operation analyses and schemes will be critical in inducing emitters to consider PCC plants as viable.

Economically oriented operational approaches are enabled by process control, which allows for tracking of the process variables affecting the economics and for the consideration of process safety constraints. The control layer is mainly responsible for driving the system towards the most recently updated plant set points. Control approaches that have been proposed for PCC include classical proportional-integral-derivative control [13,16] as well as several formulations involving linear model predictive control (MPC) [17,18]. In contrast to linear MPC, nonlinear MPC (NMPC) [19–21] is beneficial for the control of systems with complex dynamics, such as those exhibited in the PCC system, as the model can provide a more accurate representation of the system phenomena; this comes with the cost of increased computational burden. Recently, machine learning techniques [22–24] been applied to the prediction of systems with complex dynamics [25] such as PCC [26,27], this offers a balance between modelling accuracy and computational tractability. Literature on PCC control is vast; a recent review on this subject can be found in [28]. A commonly proposed approach to achieve control flexibility in this system is through the manipulation of heating duty [13,16–19], which can enrich or dilute the PCC solvent as required but requires steam to be taken from the power

plant. An aspect that has not been considered for control is the use of makeup streams to achieve the same flexibility while abating the use of steam that could otherwise be used for power generation.

For feedback control to be practically implementable, the plant states must be fully measurable or observable. Accordingly, state estimation is used as many system states required by the controller cannot be measured online; this is particularly important in complex systems that include several states. In comparison to the control literature for PCC, the available state estimation literature is sparse. Notably, [18] and [29] paired a KF with linear and nonlinear MPCs for control of the PCC, respectively. The latter used a mechanistic control model and required the measurement of 74/110 system states and very low process noise for successful state estimation. Moreover, [30] used moving horizon estimation (MHE) to perform fault diagnosis, whereby the PCC absorber was decomposed into spatial subsystems (i.e., it was decomposed into five stages, each with its own estimator) and only gas temperatures were measured. MHE is an advanced estimation scheme well-suited to deal with nonlinearities and constraints. Its use in PCC, which is nonlinear and often constrained, could allow for more accurate and reliable state estimates than KF, leading to a more effective control layer. Despite these recent advances in the state estimation literature for the PCC process, a full MHE implementation, which requires a realistically achievable number of measurements (i.e., lower than the 74 required by the KF in [29]) without model decomposition, has yet to be implemented and engaged within a broader operational scheme (i.e., with MPC and RTO) for PCC plants. More broadly, there is also a gap for an integrated operating scheme that addresses the economic, control, and estimation problems simultaneously.

The ability to estimate plant states, which can subsequently be fed to a controller to steer the system towards desirable operating points, enables the implementation of optimal operation approaches. These can be put into two categories, both of which could use mechanistic process models: economic MPC (EMPC), in which an optimal control problem is formulated with an economic objective, thus providing economically-driven control actions directly to the plant; and real-time optimization (RTO), in which a steady-state problem is formulated with an economic objective, hence providing steady state set points that are passed to a control layer and are updated when significant disturbances occur. While RTO is a steady-state method, EMPC is inherently dynamical; as such, it often requires stabilization (e.g., terminal constraints/cost) and intensive computational effort per sampling interval [31], making it difficult to implement online. The economically optimal operational approaches for PCC are summarized in Table 1:

Table 1: Summary of literature pertaining to the economically optimal operation of PCC processes.

Ref.	Approach	Findings	Drawbacks
Chan and Chen, 2018 [31]	EMPC	Approach for MEA-based plant provided ~10% cost reduction over a constant operating point. Disturbances in flue gas quality and utility costs were considered.	Full state access was assumed (no estimation). Only solvent and utility costs considered. MEA makeup manipulated.
Decardi-Nelson, Liu and Liu, 2018 [32]	EMPC/ RTO	Approach for MEA-based plant provided ~6% cost savings over a constant operating point. EMPC and RTO were compared. RTO performance was found to approach EMPC performance if executed frequently. Disturbances in flue gas flowrate and steam price were considered.	Full state access was assumed (no estimation). Only carbon tax and thermal costs considered. Reboiler duty manipulated.
Patrón and Ricardez-	RTO/ NMPC/ KF	Approach for MEA-based plant provided ~10% cost reduction over a 'no RTO' (no set	KF requires little noise and many measurements. Only solvent, carbon tax, and

Sandoval, 2020 [29]		point update) scenario in diurnal operation and varying carbon tax scenarios.	pumping costs considered. Flowrate into absorber manipulated.
Akula et al., 2021 [33]	RTO	Approach for MEA-based plant provided an analysis of the optimal steady-state operating point in part-load, full-load, and varying flue gas composition scenarios.	Dynamics were not considered (i.e., no control/estimation). Only pumping, heating, and cooling costs considered. Reboiler duty manipulated.

The following conclusions can be made from this review of the economically optimal operation literature: 1) the existing studies are tailored specifically to MEA-based plants, 2) the respective economic functions considered in the previous studies ignored key aspects of the process economics in their cost function (e.g., [32] included thermal and carbon tax costs but ignored solvent costs), 3) none of the previous studies have manipulated both MEA and water makeup streams to achieve solvent enrichment/dilution ([31] only manipulated the MEA makeup), 4) only one of the studies [28] addressed the state estimation problem but did so under restrictive assumptions (i.e., small noises and 74 measurements, including various composition which would be impractical to measure online). This elucidates the following gaps in the literature: 1) the need for a generic operating scheme that can be applied to a general class of PCC plants to achieve economically optimal operation while promoting CO_2 removal, 2) the need for an economic function that is comprehensive through its inclusion of all significant economic aspects of PCC, 3) an advanced model-based control scheme that can manipulate PCC plants flexibly without solely relying on the energy-intensive reboiler, 4) an advanced model-based state estimation scheme that is accurate and reliable in terms of the measurements required.

The contributions of this study are as follows:

1) Jointly address the economic operation, control, and state estimation for general PCC plants operating downstream from fuel-fired power plants by using a mechanistic process model in RTO, NMPC, and MHE layers, respectively. To the authors' knowledge, this is the first operational scheme in PCC (or indeed any CCS) to use an optimal three-layer operational approach and a mechanistic process model in each of the manufacturing layers. The mechanistic process model is well-suited to perform this task as it produces highly accurate decisions and predictions in each of the layers, which results in an effective operation scheme in closed loop. Moreover, RTO is suitable for this system as it is computationally efficient and produces economically attractive set points.

2) Introduce a generalized economic objective function that can be adapted for all PCC plants (i.e., with different designs, solvents, prices, etc.). The proposed economic function brings together the aforementioned aspects of the economics for the first time (i.e., energy, chemical, utility), and includes novel carbon economy factors (i.e., social cost and recoups). A detailed economic model is key when many competing incentives can affect process costs such as in PCC. Using the proposed economic model, the RTO can provide realistic economically optimal steady states for different upstream power plant operations at which to maintain key variables while also incentivizing the removal of CO_2.

3) Design a centralized multivariable control approach for the PCC plant, which enables large disturbances from the power plant to be handled through the manipulation of makeup streams. The proposed NMPC control scheme is advantageous since the PCC system exhibits strong interactions between the manipulated and controlled variables.

In addition, the manipulation of both makeup streams, which is a first in this the present study, helps in diluting/concentrating removal solvents to effectively manipulate the removal of CO_2.

4) Introduce the first model-based advanced estimation to be used within a control framework for PCC plants. The scheme consists of an MHE formulation that requires a realistic/accessible set of measurements and can accommodate for a substantial amount of noise. The mechanistic model applied to the estimation layer accurately captures the past process dynamics, which helps in producing highly accurate state estimates for the nonlinear dynamics exhibited in PCC.

This economic operation scheme is applied to the absorber section of a pilot-scale PCC plant with approximations of the stripper section effects. The plant and scheme are subjected to scenarios that would occur in PCC plants owing to changes in the power plant including: A) co-firing of coal and biomass, such that the economics of each fuel under the new objective function can be observed; B) diurnal variation in flue gas quantities, which allows for assessment of the scheme performance under upstream power plant load variation; and C) price changes, such that the dependence of the economics on prices can be assessed. These scenarios are primarily assessed using their process economics as it pertains to the improvements in steady-state PCC cost and the associated energy penalty on the power plant imposed by the RTO.

This paper is organized as follows: section 2 presents generalized RTO formulation, NMPC, and MHE formulations; section 3 briefly reviews the absorber model and gives a detailed outline of the tank model for the pilot-scale PCC plant case as well as model validation; section 4 presents the specifics of the proposed scheme as applied to the pilot PCC plant; section 5 presents the results of the outlined test scenarios performed on the proposed scheme; and section 6 gives concluding remarks as well as directions for future work.

2. Proposed economic operation scheme and formulations

PCC plants are subject to frequent disturbances, which impact the process operation and economics. Operating conditions that were once economically optimal become suboptimal thereby rendering the process set points outdated. For instance, a PCC system that requires a high CO_2 removal set point to maintain good process economics could be subject to a decrease in CO_2 composition in the flue gas. This disturbance would allow for a decrease in the removal set point because of the lower throughput of CO_2. In this situation, the lower removal set point would be an opportunity for savings from chemical materials (i.e., water and solvent consumption) as well as energy costs, which inflate the removal rate. As indicated above, economic detriment posed by the PCC to the upstream power plant remains the main factor in preventing adoption of this technology; thus, economical operating schemes are paramount in inciting its widespread uptake. Figure 1 outlines the flow of information of the proposed scheme, described next, which aims to operate the process in an economically optimal fashion while maintaining the closed-loop operation of the plant on target and using few available online measurements.

The PCC plant is subject to disturbances denoted as $\boldsymbol{d_t}$ in Figure 1. These disturbances cause the plant to deviate from its predefined set points, which can have economic and safety implications. An advanced model-based controller such as NMPC can be deployed to ensure that the plant meets its operational targets despite the occurrence of these disturbances. At every sampling interval, the NMPC requires access to the full set of model states (i.e., concentrations, temperatures, hold ups); however, only a small portion of the states are often available for online measurements ($\boldsymbol{z_t}$),

which are typically corrupted with measurement noise $\boldsymbol{v_t}$. The lack of a full set of measured states to provide to the NMPC requires the use of a reliable state estimation framework that can operate for a wide range of operating conditions. In this work, MHE is employed since it can deal with process nonlinearities that are present in PCC. MHE comprises a dynamic optimization problem that uses the available noisy measurements ($\boldsymbol{z_t + v_t}$, as shown in Figure 1) to provide an estimate of the full set of plant states ($\boldsymbol{\hat{x}_t}$) at the current time. These estimates are computed such that the model state predictions are consistent with historical process measurements and estimates.

Once the set of states are estimated by the MHE, they are fed to the NMPC as initial conditions ($\boldsymbol{\hat{x}_{t,NMPC} = \hat{x}_{t,MHE}}$, as shown in Figure 1) to solve another dynamic optimization problem that determines control actions for the plant. The control actions are computed such that the controlled variables are regulated towards their set points by the process manipulated variables ($\boldsymbol{u_{t+1}}$, as shown in Figure 1). The manipulated variables are subsequently passed to the plant, and after a time interval has elapsed (i.e., $t \leftarrow t + 1$), the procedure of measurement, estimation, and control is repeated. This repeated cycle provides constant feedback to the NMPC via the MHE so that the plant behaviour is properly regulated.

On a longer timescale, as the process operation varies significantly owing to the disturbances, operating points must be updated as noted above. When the closed-loop operation of the plant is at steady state, the RTO is triggered such that a new economically optimal steady-state operating point is defined for the plant. The RTO uses steady-state measurements ($\boldsymbol{z_t + v_t}$) to provide updated controlled variables set points to the NMPC ($\boldsymbol{Y_{sp} = Y_{RTO}}$, as depicted in Figure 1). These set point updates cause the NMPC layer to operate the system dynamically such that the updated controlled variables are eventually reached. Upon reaching these set points, the plant will be operating in an economically optimal manner until a new disturbance occurs. Each of the components of Figure 1 is discussed in further detail in the following subsections.

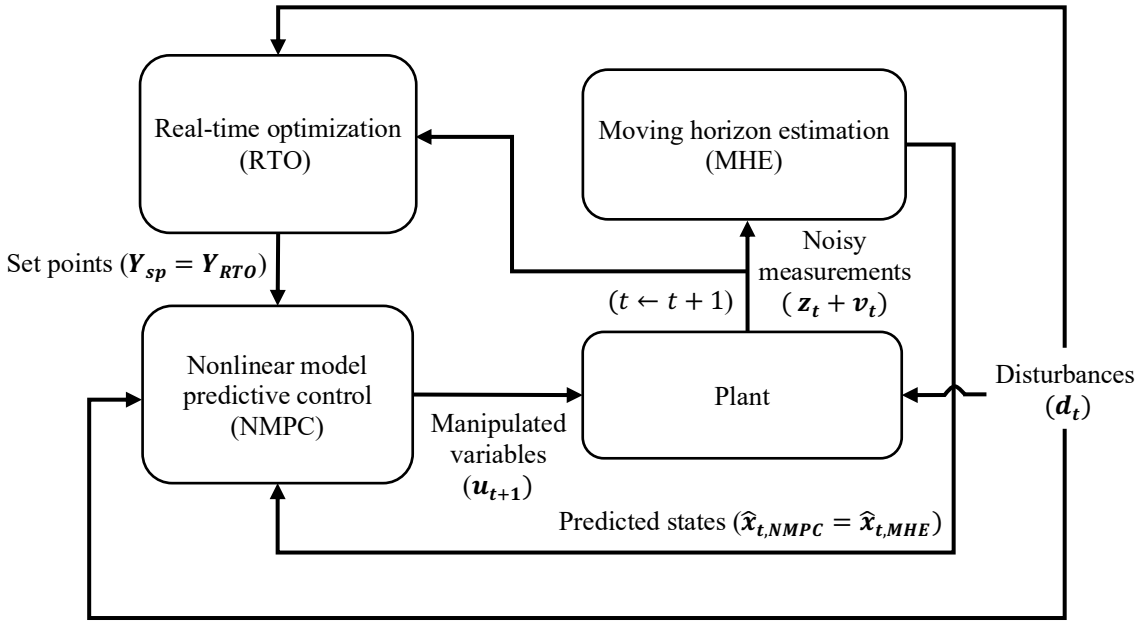

Figure 1: Proposed scheme for PCC plants

2.1. RTO formulation

A novel RTO economic function for a general PCC process is introduced along with the RTO formulation, which provides updated set points to the NMPC as depicted in Figure 1. The RTO formulation proposed for PCC plants is as follows:

$$\begin{aligned}
&\min_{\boldsymbol{Y}} \sum_i P_{chem,i}\dot{m}_{chem,i}^{mkup} + \zeta P_{sales}\dot{m}_{CO_2}^{cap} + P_{CO_2}\dot{m}_{CO_2}^{vent} + \sum_j P_{energy,j}Q_{energy,j} + \sum_k P_{H_2O}\dot{m}_{H_2O,k} \\
&s.t. \\
&\boldsymbol{f_s}(\boldsymbol{x},\boldsymbol{u},\boldsymbol{d},\boldsymbol{y},\boldsymbol{Y}) = \boldsymbol{0} \\
&\boldsymbol{g_s}(\boldsymbol{x},\boldsymbol{u},\boldsymbol{d},\boldsymbol{y},\boldsymbol{Y}) \leq \boldsymbol{0} \\
&\boldsymbol{Y^l} \leq \boldsymbol{Y} \leq \boldsymbol{Y^h} \\
&\boldsymbol{u^l} \leq \boldsymbol{u} \leq \boldsymbol{u^h}
\end{aligned} \tag{1}$$

where $\boldsymbol{f_s}: \mathbb{R}^{N_x} \times \mathbb{R}^{N_u} \times \mathbb{R}^{N_d} \times \mathbb{R}^{N_y} \times \mathbb{R}^{N_Y} \longrightarrow \mathbb{R}^{N_x}$ is the PCC model at steady state, which maps the disturbance variables ($\boldsymbol{d} \in \mathbb{R}^{N_d}$) to the steady states ($\boldsymbol{x} \in \mathbb{R}^{N_x}$), manipulated variables ($\boldsymbol{u} \in \mathbb{R}^{N_u}$), algebraic variables ($\boldsymbol{y} \in \mathbb{R}^{N_y}$), and the controlled variables ($\boldsymbol{Y} \in \mathbb{R}^{N_Y}$). $\boldsymbol{g_s}: \mathbb{R}^{N_d} \times \mathbb{R}^{N_x} \times \mathbb{R}^{N_u} \times \mathbb{R}^{N_y} \times \mathbb{R}^{N_Y} \longrightarrow \mathbb{R}^{N_g}$ denotes the set of inequality constraints (aside from upper and lower bounds) that determine the feasible region for the PCC plant in the RTO framework. $\boldsymbol{Y^l}$ and $\boldsymbol{Y^h} \in \mathbb{R}^{N_Y}$ are the lower and upper bounds for the controlled variables, respectively, whereas $\boldsymbol{u^l}$ and $\boldsymbol{u^h} \in \mathbb{R}^{N_u}$ are the lower and upper bounds for the manipulated variables, respectively. The RTO procedure can also involve a parameter estimation step, which uses the available measurements to estimate uncertain parameters; this step is omitted for brevity.

The objective function lumps the major economic factors present in the PCC process into five categories. Firstly, it considers the fresh feeds of chemical solvents 'i' used for absorption, which are often expensive (e.g., CANSOLV, KS-1, AMP/PZ, etc., [11]). These chemicals typically perform the removal of the CO_2 via various reactive absorption mechanisms. As such, the first (chemical) cost term is comprised of the fresh feeds of the various chemicals being fed to the process ($\dot{m}_{chem,i}^{mkup}$) along with their respective market price ($P_{chem,i}$).

The second term (sales) represents the recoups that can be made by selling the captured CO_2. This is the first time that this cost has been considered explicitly in an economic optimization function for PCC (it has previously only been considered in technoeconomic analyses e.g., [35]). As CCS technologies become increasingly mature, a competitive market for the captured product will emerge, thus allowing for emitters to recover some of the losses incurred by the capture process. This term consists of the price of selling captured CO_2, (P_{sales}) and the capture rate of CO_2 ($\dot{m}_{CO_2}^{cap}$). This 'price' is negative as this term represents a profit (contrasted to the other terms which represent a cost). $\zeta \in [0,1]$ denotes an efficiency factor that quantifies the portion of the total CO_2 captured that can be sold.

The third term (carbon) consists of the social cost of carbon (SCC), which includes the market cost of emitting CO_2 as well the non-market negative externalities of emissions. Negative externalities are costs not typically borne by the emitter but by a third-party (e.g., the associated effects on human and environmental health and their remediation) and are largely ignored within most carbon tax frameworks. By taking the social cost into account, the economic burden of these externalities is shifted back to the emitter, thus representing a larger penalty than a carbon tax. This term consists of the price of emitting carbon (P_{CO_2}) and the CO_2 emission rate ($\dot{m}_{CO_2}^{vent}$) via the vent gas. This is the first time that SCC is used in the economic optimization of a PCC process to provide a more complete perspective of the

effects of emissions. Past studies have used simple carbon tax prices [29,33]; however, a carbon tax will under-incentivize the removal of CO_2 as it ignores the negative externalities caused by the emission of CO_2.

The fourth (energy) term is comprised of all the energy-intensive units 'j' within the plant (e.g., reboilers, blowers, pumps, preheaters, etc.). This cost term is typically the most significant within PCC plant and is, in fact, the reason why their widespread uptake remains nascent. It consists of the unit price of energy (e.g., steam, electricity, etc., $P_{energy,j}$) as well as the energy consumption requirements (e.g., duty, load, etc., $Q_{energy,j}$). As the proposed scheme does not include a model of the power plant, this energy cost considers the energy requirements of the PCC plant but not its potential effects on the associated energy generation (i.e., the economic effect of taking steam for the PCC that could otherwise be used to produce energy). While the effects of PCC on the power plant are not considered in the RTO decisions, they are nonetheless assessed to ensure that the PCC is hindering the power generation unduly; this is discussed in the following sections.

The fifth (water) term is comprised of all the water-consuming units 'k' within the plant (e.g., makeups, condenser, etc.). This cost term is typically not very significant for PCC plants owing to the low price of water but it is included for completeness. This term consists of the price of water (P_{H_2O}) as well as the water consumption by individual units ($\dot{m}_{H_2O,k}$).

Using the economic function described in formulation (1), the RTO determines the set points for the controlled variables ($\boldsymbol{Y_{sp} = Y_{RTO}}$) to pass to the controller, as shown in Figure 1. These set points will change significantly as disturbances ($\boldsymbol{d}$) occur. The RTO problem is triggered when the PCC system reaches steady state; to detect steady state, there are various criteria that can be applied as outlined by [36].

2.2. NMPC Formulation

The NMPC uses the dynamic process model to determine the control actions that are used by the plant at every sampling interval to regulate the process. For PCC plants, which are highly nonlinear, an NMPC rather than a linear MPC is preferred to provide quick control actions with little offset.

In NMPC, the manipulated variables act to regulate the controlled variables to the steady-state set points supplied by the RTO ($\boldsymbol{Y_{sp}} \in \mathbb{R}^{N_Y}$) in the presence of disturbances. The control actions are computed by solving an optimal control problem on a future time horizon whereby the sum of squared errors between the controlled variables and their set points as well as the squared changes in the manipulated variables are minimized. These, respectively, minimize set point offset and manipulated variable movement. To solve this dynamic problem, the mechanistic model requires the full set of process states as initial conditions, which acts as feedback from the plant to the controller; these are estimated by the MHE estimation framework based on the available plant measurements. With the initial conditions, the NMPC model is used to predict the future process behaviour on the future horizon $i \in \{1, \dots, P\}$ (i.e., $\hat{\boldsymbol{x}}_{\boldsymbol{t+1}}, \dots, \hat{\boldsymbol{x}}_{\boldsymbol{t+P}}$) and determine manipulated variable trajectories on the horizon $j \in \{1, \dots, C\}$ (i.e., $\boldsymbol{u_{t+1}}, \dots, \boldsymbol{u_{t+C}}$) that are optimal for the given objective function; these horizons are depicted as $t + P$ and $t + C$ in Figure 2, respectively. The first of these manipulated variables values (i.e., $\boldsymbol{u_{t+1}}$, shown at the $t + 1$ marker Figure 2) is passed to the plant, which is then operated for a sampling interval ($\Delta t = 1$ interval, as depicted in Figure 1). At this new interval, the NMPC is re-computed, thus moving the horizon forward in time and creating a 'moving horizon'. The NMPC formulation solved at every time instance is as follows:

$$\min_{\boldsymbol{u_{t+j}}\forall j\in\{1,\dots,C\}} \sum_{i=1}^{P} \left\|\widehat{\boldsymbol{Y}}_{\boldsymbol{t+i}} - \boldsymbol{Y_{sp}}\right\|_{\boldsymbol{Q_c}}^2 + \sum_{j=1}^{C} \left\|\Delta \boldsymbol{u_{t+j}}\right\|_{\boldsymbol{R_c}}^2$$

$$s.t.$$

$$\begin{aligned}
&\boldsymbol{f_d}\left(\widehat{\boldsymbol{x}}_{\boldsymbol{t+i}}, \boldsymbol{u_{t+j}}, \boldsymbol{d_{t+i}}, \widehat{\boldsymbol{y}}_{\boldsymbol{t+i}}, \widehat{\boldsymbol{Y}}_{\boldsymbol{t+i}}\right) = \widehat{\boldsymbol{x}}_{\boldsymbol{t+i+1}} && \forall i \in \{0,\dots,P-1\},\ \forall j \in \{0,\dots,C\} \quad (2)\\
&\widehat{\boldsymbol{x}}_{\boldsymbol{t,NMPC}} = \widehat{\boldsymbol{x}}_{\boldsymbol{t,MHE}} &&\\
&\boldsymbol{g_d}\left(\boldsymbol{x_{t+i}}, \boldsymbol{u_{t+j}}, \boldsymbol{d_{t+i}}, \widehat{\boldsymbol{y}}_{\boldsymbol{t+i}}, \widehat{\boldsymbol{Y}}_{\boldsymbol{t+i}}\right) \le \boldsymbol{0} && \forall i \in \{0,\dots,P\},\ \forall j \in \{0,\dots,C\}\\
&\boldsymbol{Y^l} \le \boldsymbol{Y_{t+i}} \le \boldsymbol{Y^h} && \forall i \in \{0,\dots,P\}\\
&\boldsymbol{u^l} \le \boldsymbol{u_{t+j}} \le \boldsymbol{u^h} && \forall j \in \{1,\dots,C\}
\end{aligned}$$

where $\|\boldsymbol{X}\|_{\boldsymbol{A}}^2$ denotes a quadratic form on vector $\boldsymbol{X} \in \mathbb{R}^{\boldsymbol{n}}$ with the weighting matrix $\boldsymbol{A} \in \mathbb{R}^{\boldsymbol{n\times n}}$. $\boldsymbol{f_d}$: $\mathbb{R}^{N_x} \times \mathbb{R}^{N_u} \times \mathbb{R}^{N_d} \times \mathbb{R}^{N_y} \times \mathbb{R}^{N_Y} \longrightarrow \mathbb{R}^{N_x}$ is the dynamic mechanistic model (not at steady state as with the RTO). Inputs to problem (2) are the initial conditions ($\widehat{\boldsymbol{x}}_{\boldsymbol{t,NMPC}} \in \mathbb{R}^{N_x}$) and disturbances ($\boldsymbol{d_{t+i}} \in \mathbb{R}^{N_d}$) whereas the outputs are the states ($\widehat{\boldsymbol{x}}_{\boldsymbol{t+i}} \in \mathbb{R}^{N_x}$), manipulated variables ($\boldsymbol{u_{t+j}} \in \mathbb{R}^{N_u}$), algebraic variables ($\widehat{\boldsymbol{y}}_{\boldsymbol{t+i}} \in \mathbb{R}^{N_y}$), and controlled variables ($\widehat{\boldsymbol{Y}}_{\boldsymbol{t+i}} \in \mathbb{R}^{N_Y}$) on their respective horizon P or C. The disturbances $\boldsymbol{d_{t+i}}$ are denoted with the time index (compared to $\boldsymbol{d}$ in the RTO) as a trajectory of disturbances is required by the NMPC; however, this trajectory in the prediction horizon is assumed to be constant (i.e., $\boldsymbol{d_t} = \boldsymbol{d_{t+1}} = \cdots$) as knowledge of the disturbances cannot be known *a priori* to their occurrence. The feedback from the plant at the beginning of the horizon 't' ($\widehat{\boldsymbol{x}}_{\boldsymbol{t,MHE}} \in \mathbb{R}^{N_x}$) is comprised of measurements and estimates made by the MHE scheme as shown at the t marker in Figure 2. The terms $\boldsymbol{Q_c} \in \mathbb{R}^{N_Y \times N_Y}$ and $\boldsymbol{R_c} \in \mathbb{R}^{N_u \times N_u}$ are weights used to tune the controller such that its performance is acceptable. $\boldsymbol{g_d}$: $\mathbb{R}^{N_d} \times \mathbb{R}^{N_x} \times \mathbb{R}^{N_u} \times \mathbb{R}^{N_y} \times \mathbb{R}^{N_Y} \longrightarrow \mathbb{R}^{N_g}$ denotes the set of inequality constraints (aside from upper and lower bounds) that can be applied to the NMPC-predicted trajectories. As with the RTO in equation (1), $\boldsymbol{Y^l}$ and $\boldsymbol{Y^h} \in \mathbb{R}^{N_Y}$ are the lower and upper bounds for the controlled variables, respectively; and $\boldsymbol{u^l}$ and $\boldsymbol{u^h} \in \mathbb{R}^{N_u}$ are the lower and upper bounds for the manipulated variables, respectively; in the future horizon.

The NMPC as described in formulation (2) provides the control actions ($\boldsymbol{u_{t+1}}$) to the plant by which the set points provided by the RTO can be tracked. It imposes dynamic operation on the plant to reject disturbances ($\boldsymbol{d_t}$) when occur and to change set points ($\boldsymbol{Y_{sp}}$) when specified by the RTO. Each execution of the NMPC problem requires feedback from the plant via the MHE such that the full set of plant states are provided as inputs at each time interval (Δt) to the NMPC framework as shown in Figure 2.

2.3. MHE formulation

As noted with the NMPC, most PCC plants (and indeed most CCS processes) exhibit a highly nonlinear behaviour; hence, the state estimation is often subject to substantial process uncertainty for which linear filters (e.g., KF) may be ill-suited. Moreover, measurements are corrupted with noise and PCC plants are subject to process constraints that must be satisfied during operation (e.g., safety bounds on temperature estimates). MHE is particularly well-suited for these types of problem as it enables the use of a detailed model to handle process nonlinearities, process constraints, and provides substantial smoothing of noise. In the proposed scheme, the MHE uses a dynamic process model to estimate the full state vector at every sampling interval ($\Delta t = 1$ interval) such that it can be supplied to the NMPC as feedback (i.e., $\widehat{\boldsymbol{x}}_{\boldsymbol{t,MHE}} \in \mathbb{R}^{\boldsymbol{N_x}}$ is used as initial conditions for the problem in equation (2)). This requires that plant measurements be supplied to the MHE at every execution such that it has updated information on the most recent (as well as past) states of the plant. In contrast to the NMPC, which makes future predictions of the process, the MHE

esimates the current process state by building a horizon N time intervals into the past, i.e., $k \in \{0, \dots, N\}$ (depicted at the $t - N$ marker in Figure 2).

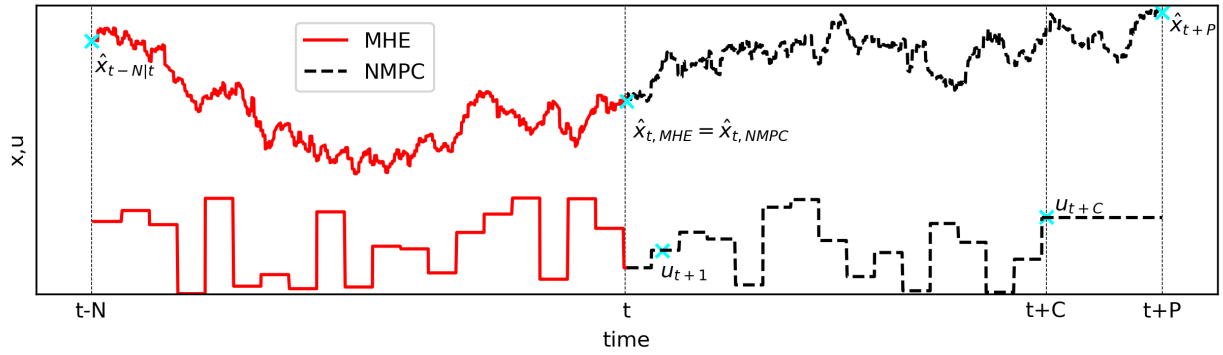

Figure 2: Relationship between MHE and NMPC. x denotes a state variable and u denotes a manipulated variable. Cyan X markers denote points of interest. Past of the process denoted in red, future of the process denotes in black.

In the past horizon, the history of the process can be reconstructed through its known measurements, estimates, and control actions; leading to a current state estimate that conforms with past plant behaviour. The MHE formulation solved at every time instance t and is as follows:

$$\min_{\substack{\hat{\boldsymbol{x}}_{t-N|t}, \boldsymbol{v}_{t-i|t}, \boldsymbol{w}_{t-i|t} \\ \forall i \in \{0,\dots,N\}}} \sum_{i=1}^{N} \left\| \boldsymbol{v}_{t-i|t} \right\|_{\boldsymbol{Q_e}}^2 + \sum_{i=0}^{N-1} \left\| \boldsymbol{w}_{t-i|t} \right\|_{\boldsymbol{R_e}}^2 + \varphi_{t-N}$$

$$s.t.$$

$$\boldsymbol{f_d}\left(\hat{\boldsymbol{x}}_{t-i|t}, \boldsymbol{u}_{t-i}, , \boldsymbol{d}_{t-i}, \hat{\boldsymbol{y}}_{t-i|t}, \hat{\boldsymbol{Y}}_{t-i|t}\right) = \hat{\boldsymbol{x}}_{t-i+1|t} + \boldsymbol{v}_{t-i+1|t} \qquad \forall i \in \{1, \dots, N\} \quad (3)$$

$$\boldsymbol{h_d}\left(\hat{\boldsymbol{x}}_{t-i|t}\right) = \boldsymbol{z}_{t-i} + \boldsymbol{w}_{t-i|t} \qquad \forall i \in \{0, \dots, N-1\}$$

$$\boldsymbol{g_d}\left(\boldsymbol{x}_{t-i|t}, \boldsymbol{u}_{t-i}, \boldsymbol{d}_{t-i}, \hat{\boldsymbol{y}}_{t-i|t}, \hat{\boldsymbol{Y}}_{t-i|t}\right) \leq \boldsymbol{0} \qquad \forall i \in \{0, \dots, N\}$$

$$\boldsymbol{Y^l} \leq, \hat{\boldsymbol{Y}}_{t-i|t} \leq \boldsymbol{Y^h} \qquad \forall i \in \{0, \dots, N\}$$

where $\boldsymbol{z_{t-i}} \in \mathbb{R}^{N_z}$ is the history of the process measurements for the past N time intervals until the time 't' at which the MHE is executed. $\boldsymbol{v_{t-i+1|t}} \in \mathbb{R}^{N_x}$ and $\boldsymbol{w_{t-i|t}} \in \mathbb{R}^{N_z}$ are the process and measurement noise terms on the past horizon, respectively; the square of these noise terms is minimized in the objective function. $\boldsymbol{h_d}$: $\mathbb{R}^{N_x} \longrightarrow \mathbb{R}^{N_z}$ is the observation model and, as with the NMPC, $\boldsymbol{f_d}$: $\mathbb{R}^{N_x} \times \mathbb{R}^{N_u} \times \mathbb{R}^{N_d} \times \mathbb{R}^{N_y} \times \mathbb{R}^{N_Y} \longrightarrow \mathbb{R}^{N_x}$ is the dynamic mechanistic process model. The inputs to problem (3) are the manipulated variable ($\boldsymbol{u_{t-i}} \in \mathbb{R}^{N_u}$), disturbance variable ($\boldsymbol{d_{t-i}} \in \mathbb{R}^{N_d}$), measurement ($\boldsymbol{z_{t-i}}$), and state ($\hat{\boldsymbol{x}}_{t-i|t}$) histories on the horizon N and the output the current system state ($\hat{\boldsymbol{x}}_{t|t} \in \mathbb{R}^{N_x}$). $\boldsymbol{Q_e} \in \mathbb{R}^{N_x \times N_x}$ and $\boldsymbol{R_e} \in \mathbb{R}^{N_z \times N_z}$ are weighting matrices for the objective function; these are inversely proportional to the process and measurement noise covariances, respectively. Both $\boldsymbol{Q_e}$ and $\boldsymbol{R_e}$ are estimated at every sampling interval based on previous estimates and measurements, respectively. As with the NMPC and RTO, $\boldsymbol{Y^l}$ and $\boldsymbol{Y^h} \in \mathbb{R}^{N_Y}$ are the lower and upper bounds for the controlled variables, respectively. $\boldsymbol{g_d}$: $\mathbb{R}^{N_d} \times \mathbb{R}^{N_x} \times \mathbb{R}^{N_u} \times \mathbb{R}^{N_y} \times \mathbb{R}^{N_Y} \longrightarrow \mathbb{R}^{N_g}$ denotes the set of inequality constraints (aside from upper and lower bounds) to which the MHE estimates must adhere. $\varphi_{t-N} \in \mathbb{R}$ denotes the arrival cost, which penalizes the MHE for truncating the horizon to a finite length, this can be estimated using a variety of filters as explored in [37].

The first (process noise) term in the objective function represents the process uncertainty within the MHE horizon. Moreover, the second (measurement noise) term represents the errors in the MHE state estimates with their associated

historical measurements within the estimation horizon. The arrival cost accounts for previous information discarded in the MHE since it was gathered before the current estimation horizon (i.e., historical information of the process prior to $t - N$). By embedding prior available measurements within the MHE problem, the objective function ensures that the current state estimates are consistent with prior state measurements. The resulting MHE state estimates for a given time interval are provided to the NMPC and used as the initial conditions to solve the corresponding optimal control problem. Hence, the future state trajectories predicted by the NMPC begin at the MHE-estimated operating point of the system (as shown where the two trajectories meet in Figure 2). Given the estimates provided by MHE at the current time interval 't' ($\hat{\boldsymbol{x}}_{\boldsymbol{t,MHE}}$), the NMPC problem provides the optimal control actions to run the process plant and perform MHE for the next time interval '$t \leftarrow t + 1$'. That is, once the new measurements are available (from the process plant), MHE uses these measurements together with the control actions provided by NMPC to estimate the states that are needed to initialize the NMPC problem. Note that inaccurate initial conditions provided by the MHE would likely result in inaccurate control actions predicted by the NMPC thus resulting in an undesirable or even unstable closed-loop operation of the system. Likewise, inaccurate control actions provided by NMPC may lead to a significant loss of performance in the MHE scheme and therefore inaccurate estimations. Thus, a high performance of both the NMPC and MHE schemes is required to avoid intensifying the errors and to achieve a proper closed-loop performance.

Using the formulations presented in this section, information is exchanged between the operational layers as depicted in Figure 1 and in Figure 2 for the NMPC and MHE schemes. The RTO provides economically optimal set point updates ($\boldsymbol{Y_{sp}}$) to the NMPC upon the occurrence of disturbances ($\boldsymbol{d_t}$). These set points are achieved by the NMPC through the manipulated variables ($\boldsymbol{u_{t+1}}$), which are used to control the plant. The NMPC is provided with the current states as feedback to determine optimal control actions; these states are estimated by the MHE ($\hat{\boldsymbol{x}}_{\boldsymbol{t,MHE}}$) using the available noisy measurements ($\boldsymbol{z_t} + \boldsymbol{v_t}$). The control/estimation procedure is repeated at every sampling interval (Δt), while the RTO procedure is performed less often when the system reaches steady state.

3. PCC absorber section case study

A general representation of the PCC process is depicted in Figure 3. There are $n_{comp} = 4$ chemical species modelled as part of the system denoted as $i = \{1: MEA, 2: CO_2, 3: H_2O, 4: N_2\}$. As shown in Figure 3, a 'lean' MEA solution enters the absorber in the liquid phase through a variable-speed pump; this solvent removes CO_2 from the gas phase within the absorber. The stream entering the bottom of the absorber is the flue gas from an upstream power plant; the CO_2 to be removed enters the system in this stream, which also contains water vapour and nitrogen gas (N_2). Within the column a reactive absorption mechanism occurs along the absorber height, whereby the liquid MEA reacts with the gaseous CO_2 to form a water-soluble salt, which is then dissolved in the solvent. A vent gas is outputted from the top of the absorber containing water, the N_2, and traces of unremoved CO_2, which is emitted into the environment. Moreover, a 'rich' amine solution is outputted from the absorber bottom containing MEA, water, and the removed CO_2. This rich stream goes through a cross heat exchanger where it is preheated before entering the top of the stripper. In the stripper, the CO_2 desorbs from the MEA via a high-temperature equilibrium reaction. Pure gaseous CO_2 is outputted through the top of the stripper through a condenser, which allows for the control of the purity of the CO_2 product; the impurities in this stream constitute the main MEA and water losses in the system. An MEA/water solution

is outputted through the bottom of the stripper for which a reboiler determines the ratio of this solvent solution that is recycled between the buffer tank and stripper; higher reboiler duty leads to increased CO_2 desorption in the stripper. The buffer tank recycle stream containing MEA, water, and traces of CO_2 goes through the cross-heat exchanger where it pre-heats the colder rich amine solution. The recycle stream then reaches the tank where it is mixed with two makeup streams of fresh water and fresh MEA such that the solution is concentrated or diluted as required. The recycled amine solution enters the buffer tank at 366.5 K [38]; thus, the tank contents are cooled using an internal coil through which water is circulated.

As shown Figure 3, PCC plants are composed of absorber and stripper sections, which provide a natural partition for operational schemes. In this study, the absorber section is primarily being studied (Figure 3, left dashed box), with some approximations on the behaviour of the stripper section reboiler (Figure 3, right dashed box). The focus was placed mainly on the absorber section as it is where the carbon capture from the flue gas occurs; thus, it is the most important unit from a processing perspective. This partition was necessary as to restrict the size (thus, the computational time) of the simulated plant as assessment of the entire plant would have been prohibitively protractive. As RTO is an inherently steady-state method, the decision was made that steady-state approximations of the stripper section were sufficient for its assessment. Accordingly, the stripper section economics (particularly those of the reboiler), which are important to the process, are considered through steady-state approximations elaborated upon in this section. Moreover, changes in the stripper section are assumed to occur as disturbances to the absorber section, elaborated upon in section 4; this way the stripper side operation and associated dynamics are considered in the present analysis. The NMPC and MHE implemented in the present case study, moreover, are quite general and could be applied in the larger context of a PCC plant scenario if the stripper section behaviour could be considered.

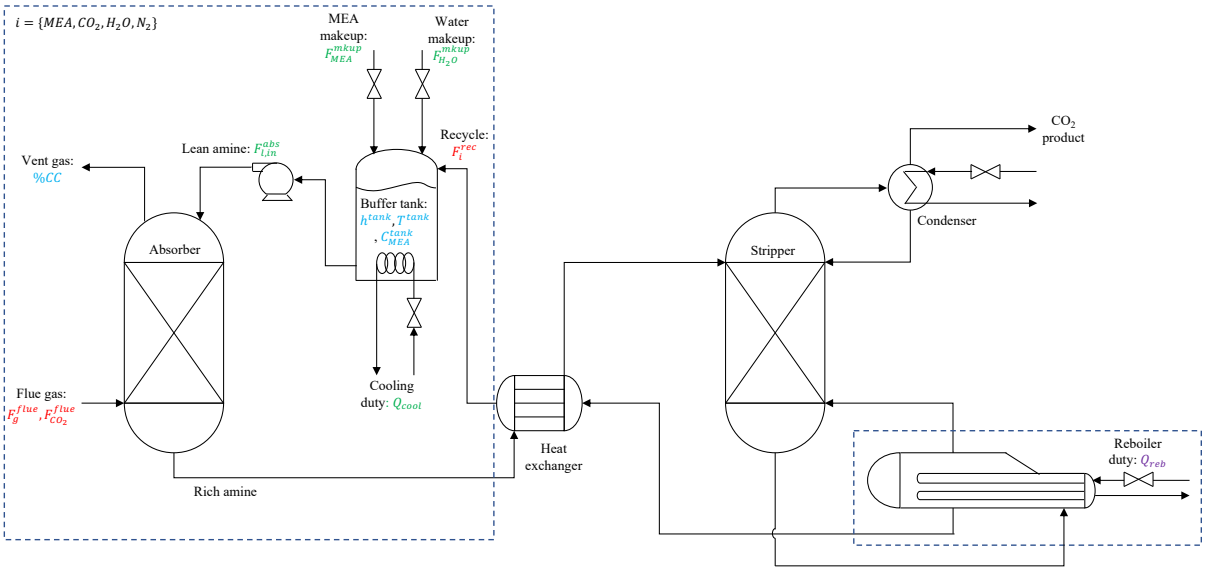

Figure 3: PCC plant. Dashed lines denote the units being considered in this study (i.e., the absorber section and reboiler). Blue font denotes controlled variables, purple font denotes additional RTO decision variables, green font denotes manipulated variables, and red font denotes disturbance variables (outlined in section 3.5).

The dynamic mechanistic model for the absorber section of the PCC plant used for the layers in this study was adapted from [38] and [39]. These are based the operating conditions for the process on the pilot plant data and configuration

from [7]. The model comprises a set of partial differential equations (PDEs), ordinary differential equations (ODEs), and algebraic equations (AEs) to describe the system dynamics and phenomena; together these are a partial differential-algebraic system of equations (PDAEs). The process model consists of material balances, energy balances, and physical property models for both units, which are presented in the next subsections. Additionally, the absorber model consists of rate equations, chemical kinetics equations, and equilibrium equations; these, along with the assumptions made in developing the absorber model, are omitted for brevity, a full description of this model is provided in [21].

3.1. Absorber section model

The absorber unit is depicted within left the dashed box in Figure 3. The position along the height of the column is denoted as z, with boundaries at the top ($z = H$) and bottom ($z = 0$). The inputs to the absorber are the lean solvent coming from the mixing tank ($z = H$) and the flue gas from the upstream power plant ($z = 0$). The outputs from the absorber are the emitted gas ($z = H$) and the rich solvent ($z = 0$) going to the stripper section. The concentrations of the chemical species within this unit vary dynamically owing to disturbances to the system (i.e., changes in inlet flowrates or compositions) and the resulting changes in the reactive process happening within the column, which lead to phase change. The internal column dynamics describing the change in concentrations of these species as a function of time (t) and position along the height of the column (z) are described by the following PDEs:

$$\frac{dC_i^l}{dt} = u_l \frac{\partial C_i^l}{\partial z} + a_w N_i \tag{4}$$

$$\frac{dC_i^g}{dt} = -u_g \frac{\partial C_i^g}{\partial z} - a_w N_i - C_i^g \frac{\partial u_g}{\partial z} \tag{5}$$

where liquid and gas species molar concentrations are denoted as C_i^l and C_i^g (mol/m^3), respectively. Species fluxes are $N_i(mol/m^2/s)$, with a positive flux denoting transfer from gas to liquid phase, and a negative direction representing the mass transfer from gas to the liquid phase; these are calculated through a mass transfer model (not shown for brevity, available in [21]). These fluxes occur on the wetted packing area $a_w(m^2/m^3)$ per unit volume. Liquid and gas fluid velocities are denoted as u_l and $u_g(m/s)$, respectively, with liquid velocity assumed to be constant because of its high density, while the gas velocity is modelled as follows:

$$\frac{\partial u_g}{\partial z} = \frac{u_g}{P}\frac{dp}{dz} + \frac{u_g}{T_g}\frac{\partial T_g}{\partial z} - \frac{a_w}{C_{tot}^g}\sum_{i=1}^{n_{comp}} N_i \tag{6}$$

where $p(kPa)$ denotes the absorber pressure, $T_g(K)$ denotes the gas phase temperature, and $C_{tot}^g = \sum_{i=1}^{n_{comp}} C_i^g$ (mol/m^3) denotes the total gas concentration. As described in [21], a linear pressure drop is assumed to happen along the absorber height; as noted by [40], this assumption is reasonable for normal operating conditions such as those exhibited in the present study.

In addition to the species phase concentration dynamics, liquid and gas phase temperature dynamics are also expected to occur owing to changes in reaction, vaporization, and interfacial thermodynamics of the absorption process as well as heat transfer with the environment. These phase temperature dynamics are modelled as follows:

$$\frac{dT_l}{dt} = u_l \frac{\partial T_l}{\partial z} - \frac{a_w}{\sum_{i=1}^{n_{comp}} c_{p,i}^{l}\, C_i^{l}} \left[h_{gl}(T_l - T_g) - \Delta H_{rxn} N_{CO_2} - \Delta H_{H_2O}^{vap} N_{H_2O} - h_{loss}(T_l - T_{amb}) \right] \quad (7)$$

$$\frac{dT_g}{dt} = -u_g \frac{\partial T_g}{\partial z} + \frac{a_w}{\sum_{i=1}^{n_{comp}} c_{p,i}^{g}\, C_i^{g}} \left[h_{gl}(T_l - T_g) \right] \quad (8)$$

where $T_l(K)$ denotes the liquid phase temperature and $T_{amb}(K)$ denotes the ambient temperature; $c_{p,i}^{l}$ and $c_{p,i}^{g}(J/mol/K)$ denote the liquid and gas phase molar specific heat capacities, respectively. $h_{gl}(J/mol/K)$ and $h_{loss}(W/m2/K)$ denoted the interfacial and absorber-to-surroundings heat transfer coefficients, respectively. $\Delta H_{rxn}(J/mol)$ and $\Delta H_{H_2O}^{vap}(J/mol)$ denote the molar heats of reaction and vaporization of water, respectively. Equations (4)–(8) comprise the differential model of the absorber unit. For brevity, the set of AEs, which includes the mass transfer, heat transfer, and equilibrium models, is omitted for brevity and can be found in [21].

3.2. Buffer tank model

As shown within the left dashed box in Figure 3, the inputs to the tank are the recycled solvent coming from the stripper as well as the fresh water and MEA makeups. The output from the tank is the lean solvent going to the absorber. Component material balances for the buffer tank account for changes in molar holdup caused by control actions on the inlet and outlet flowrates. Moreover, changes in molar holdup also occur upon disturbances in the recycled flowrates coming from the stripper section as depicted in Figure 3. Nitrogen is assumed to be insoluble in the amine solvent; thus, the buffer tank does not contain this component as in the absorber, i.e., $n_{tank} = n_{comp} - 1$. The material balances for the tank are differential molar balances for each soluble component where no reaction is taking place and the well-mixed assumption holds (stirred tank). The molar holdups are modelled as follows:

$$\frac{dn_{MEA}^{tank}}{dt} = F_{MEA}^{rec} + F_{MEA}^{mkup} - F_{MEA,out}^{tank} \quad (9)$$

$$\frac{dn_{CO_2}^{tank}}{dt} = F_{CO_2}^{rec} - F_{CO_2,out}^{tank} \quad (10)$$

$$\frac{dn_{H_2O}^{tank}}{dt} = F_{H_2O}^{rec} + F_{H_2O}^{mkup} - F_{H_2O,out}^{tank} \quad (11)$$

where F_{MEA}^{mkup} and $F_{H_2O}^{mkup}(mol/s)$ denote the fresh MEA and water flowrates, respectively. $n_i^{tank}(mol)$ denotes the tank holdup component moles. $F_{l,in}^{tank} = \sum_{i=1}^{n_{tank}} F_i^{rec}$ and $F_{l,in}^{abs} = \sum_{i=1}^{n_{tank}} F_i^{out}\ (mol/s)$ (as shown in Figure 3) denote the total recycled and tank outlet molar flowrates of species i, respectively.

In addition to the component molar balances, an overall material balance is required to model the tank's holdup as it can also change significantly because of the control actions taken to regulate the PCC system and due to changes in the recycled stream. For instance, a control action may impose an increase in the makeup flowrates which, if not adequately accounted for in the outlet flowrate, may cause the tank level to continually rise. Tracking the tank's liquid level is a necessary safety requirement to avoid overflows or emptying of the tank (i.e., for inventory management). The inventory requirements of the tank must be coordinated with the removal requirements of the absorber (i.e., changing the makeup flowrates may affect the liquid level while also affecting the amount of absorption occurring). Hence, a centralized multi-variable controller such as NMPC is well suited to handle this interaction. This balance is

performed under the assumption of constant inlet liquid densities in the makeup streams, which are valid as inlet stream are assumed to have constant compositions and temperatures. In contrast, the recycle and outlet density stream densities are modelled using the physical property models presented in the next section, as the composition of these streams may vary due to changes in the operation of the stripper section. As such, the tank liquid level is modelled as follows:

$$A^{tank}\frac{dh^{tank}}{dt} = \frac{F_{l,in}^{tank}}{\rho^{rec}} + \frac{F_{MEA}^{mkup}}{\rho_{MEA}} + \frac{F_{H_2O}^{mkup}}{\rho_{H_2O}} - \frac{F_{l,in}^{abs}}{\rho^{tank}} \tag{12}$$

where $h(m)$ denotes the tank liquid level and $A^{tank}(m^2)$ denotes the tank cross-sectional area. ρ^{rec}, ρ_{MEA}, ρ_{H_2O}, and $\rho^{tank}(mol/m^3)$ denote the total recycle, fresh MEA, fresh water, and total outlet stream molar densities, respectively. In addition to the component and overall material balances, an energy balance is required for the tank. Within this unit, streams of different temperatures are mixed, and cooling is applied. Hence, temperature tracking is needed because thermodynamic changes in the tank can lead to changes in the removal rate of the subsequent absorber unit. The temperature changes within the tank are modelled as follows:

$$\left(\sum_{i=1}^{n_{tank}} c_{p,l,i}^{tank} n_i^{tank}\right)\frac{dT^{tank}}{dt} = F_{total}^{rec} c_{p,l}^{rec}(T^{tank} - T_l^{rec}) + F_{MEA}^{mkup} c_{p,l,MEA}^{mkup}(T^{tank} - T_{MEA}^{mkup}) + F_{H_2O}^{mkup} c_{p,l,H_2O}^{mkup}(T^{tank} - T_{H_2O}^{mkup}) + Q_{cool} \tag{13}$$

where $c_{p,i}^{tank}(J/mol/K)$ denotes the tank component specific molar heat capacities. $T^{tank}(K)$ denotes the bulk tank temperature while $T_l^{recycle}$, T_{MEA}^{mkup}, and $T_{H_2O}^{mkup}(K)$ denote the inlet recycled, fresh MEA, and fresh water temperatures, respectively. Likewise, $c_{p,l}^{rec}$, $c_{p,l,MEA}^{mkup}$, and $c_{p,l,H_2O}^{mkup}(J/mol/K)$ denote the specific molar heat capacities of the recycled, fresh MEA, and fresh water streams, respectively. $Q_{cool}(W)$ denotes the cooling duty supplied to the tank through a coil.

3.3. Physical properties and process design characteristics

Table 2 contains physical property models, parameters, and design characteristics associated with the absorber model outlined in section 3.1. The physical property models, parameters, and design characteristics associated with the algebraic model can be found in [21].

Table 2: Physical property and design characteristics for the absorber model

Physical Property	**Value**	**Source**
Wetted area (m^2/m^3)	a_w	[39]
Liquid component heat capacity ($J/mol/K$)	$c_{p,l,i}$	[41]
Gas component heat capacity ($J/mol/K$)	$c_{p,g,i}$	[41]
Ambient temperature (K)	$T_{amb} = 297.6$	[39]
Absorber-surroundings heat transfer coefficient ($W/m^2/K$)	$h_{loss} = 4{,}300$	[42]
Molar heat of reaction (J/mol)	$\Delta H_{rxn} = 48{,}000$	[42]
Molar heat of vaporization (J/mol)	$\Delta H_{H_2O}^{vap} = 82{,}000$	[43]
Design Characteristics		

Internal diameter (m)	$D^{abs} = 0.43$	[39]
Packing height (m)	$h^{abs} = 6.1$	[39]
Packing type	IMTP #40	[39]

Furthermore, Table 3 contains physical property models, parameters, and design characteristics associated with the tank model described in section 3.2.

Table 3: Physical property and design characteristics for the tank model

Physical Property	**Value**	**Source**
Stream heat capacity ($J/mol/K$)	$c_{p,l}$	[41]
Recycled stream molar density (mol/L)	ρ^{rec}	[44]
Tank liquid molar density (mol/L)	ρ^{tank}	[44]
MEA molar density (mol/L)	$\rho_{MEA} = 5.05 \times 10^{-5}$	Aspen Property Package
Water molar density (mol/L)	$\rho_{H_2O} = 1.87 \times 10^{-5}$	Aspen Property Package
Design Characteristics		
Internal diameter (m)	$D^{tank} = 2$	[39]
Height (m)	$h^{tank} = 2$	[39]

3.4. Stripper section approximations

For the RTO layer to find an economically optimal point, approximations regarding the steady-state stripper section behaviour are made herein for a more realistic representation of the process and its economics. These additional equations were included as part of the RTO model to consider the stripper-side reboiler steam and solvent depletion costs.

The largest cost in the PCC plant is incurred by the steam supplied to the stripper section reboiler, which is energy-intensive and often draws the required heating steam from the upstream power plant. To consider the reboiler cost, simulated steady-state data between reboiler duty and lean loading from [38] was correlated to yield:

$$LL = a_{reb} + b_{reb} Q_{reb} \tag{14}$$

where $LL(mol/mol)$ denotes the lean loading in the recycled stream and $Q_{reb}(W)$ denotes stripper-side reboiler duty as shown in Figure 3. To correlate the data in this range, a linear model was found to accurately fit the data available with $R^2 = 0.97$ (see Figure A1 in Appendix A), thus not requiring a more sophisticated regression model. In this case, the nominal reboiler duty value of $153{,}600\ W$ corresponds to the nominal operation outlined in [38] and the data were within $\pm 5\%$ of this nominal value. A sensitivity analysis performed by [38] also established that the $\pm 5\%$ range provides ample flexibility for the reboiler to affect the lean loading (i.e., the loading is very sensitive to the reboiler duty and this range of heat duties varies the loading from ~ 0.23 to $\sim 0.32\ mol/mol$, which is a typical range for a pilot-scale PCC unit). Accordingly, the reboiler duty (Q_{reb}) was also constrained within this range in the RTO, where it becomes an additional decision variable. The reason for inclusion of reboiler duty as a decision variable in the RTO through the simplified model in equation (14) was to consider the significant reboiler cost and to understand its effect on the optimal RTO-determined controlled variables.

Solvent depletion also occurs in the stripper section due to the condenser (top right of Figure 3), which outputs some solvent with the purified CO_2. The absorber section does not contain the condenser; thus, no solvent depletion is explicitly being accounted for in the RTO model. The depleted MEA and water, while not as expensive as the reboiler

steam, need to be considered so that the system has incentive to supply makeups at steady state; thus, necessitating the modelling of solvent depletion by further approximating the behavior in the stripper section. If depletion were not considered in the absorber section it would be assumed that all the solvent can be regenerated and remain in the system; in this case, the RTO would not have incentive to feed fresh makeups at steady state owing to the high cost of the solvent chemicals (particularly MEA); this situation would be unrealistic. Accordingly, additional equations were added to model the steady-state depletion of MEA and water in the stripper and to connect the enrichment effect of the reboiler in equation (14) to the recycled stream flowrates. These equations were designed rather than fitted, such that they accounted for the contributions made by all 'fresh' inlets of the depleting species (i.e., the makeup MEA and water as well as flue gas water content). In the absence of data regarding this behaviour, the depletion was assumed to increase proportionally to the fresh feeds provided and subsequently approach constant depletion as the fresh feeds approach their nominal value; this behaviour was approximated using exponential functions for use within the RTO optimization problem.

Together with the reboiler approximation in equation (14), the RTO steady-state stripper is approximated to affect the recycle stream going from the stripper into the tank as follows:

$$F_{MEA}^{rec} = a_{MEA} + F_{MEA}^{mkup} - b_{MEA} exp(c_{MEA} F_{MEA}^{mkup}) \tag{15}$$

$$F_{CO_2}^{rec} = F_{MEA}^{rec} LL = F_{MEA}^{rec}(a_{reb} + b_{reb} Q_{reb}) \tag{16}$$

$$F_{water}^{rec} = a_{H_2O} + F_{H_2O}^{mkup} + y_{H_2O}^{flue} F_g^{flue} - b_{H_2O} exp(c_{H_2O}(F_{H_2O}^{mkup} + y_{H_2O}^{flue} F_g^{flue})) \tag{17}$$

where the parameters for equations (15)–(17) are listed in Table 4.

Table 4: Additional RTO model parameters.

i	a_i	b_i	c_i
Reboiler	1.19	-5.94e-6	-
MEA	3.2096	3.2096	-55000
Water	27.68	27.68	-5000

Due to the lack of data regarding species depletion in this specific pilot-scale system, the constants for the recycled stream parameters in equation (15) and (17) were designed such that the depletion follows the behaviour expected in a complete PCC plant. That behaviour is as follows: the MEA recycled from the absorber depletes exponentially to zero as less makeup MEA is added since this stream is the only source of fresh MEA into the system. In contrast, the recycled water depletes exponentially to a constant value specified by the flue gas water content as fresh water enters the system through both the makeup and flue gas streams. The pre-exponential coefficient for MEA (a_{MEA}) was chosen such that the recycle flowrates were effectively zero if no fresh feeds were provided, while the decay rate (b_{MEA}) was chosen to approximate linear increases in depletion that reach an asymptote as the makeup stream approaches its nominal value, this behaviour can be seen in Figure A2a in Appendix A. For consistency, the behaviour of the water recycle was also modelled with an exponential function. However, since there are two fresh water streams (i.e., within the flue gas and the makeup stream), there will always be water in the recycled stream (as water vapour is a by-product

of combustion). As such, the pre-exponential and decay rates for water (a_{water}, b_{water}, respectively) were chosen such that the water content in the recycle would increase approximately linearly with increased makeup, as shown in Figure A2b in Appendix A. The behaviour approximated herein inherently assumes that the condenser duty (hence the depletion) remains constant. In principle, the condenser duty would be one of the manipulated variables in the stripper section, but this unit is out of the scope of the present study as noted previously.

Note that these correlations approximate the steady-state effect of the reboiler and condenser on the makeup streams and do not attempt to capture dynamics. To account for the impact of these correlations on the recycle stream in the transient domain, a ramp disturbance is assumed to occur such that the recycled stream flowrate and composition are updated from their pre-RTO values to RTO-optimized values; these are described in detail in the following sections. The assumption of the recycle stream as a ramp is made here to reflect a typical operating condition of the stripper section. Note that the proposed operational framework is not limited to this assumption and can be extended to consider other profiles entering the absorber section from the recycle stream. With the treatments of stripper section effects as disturbances; the important effect of the stripper section on process dynamics is not disregarded.

3.5. Model solution and nominal operation

The set of PDAEs representing the PCC absorber section presented previously require the inputs outlined in Table 5 whereby the steady-state version requires only boundary conditions, and the dynamic version requires initial and boundary conditions. The models are implemented in the Pyomo environment, an optimization modelling package for PYTHON [45]. The absorber model is discretized in the axial (z) domain in the steady-state version while additional discretization in the time (t) domain is required in the dynamic model. This enables the differential equations comprising the continuous time/space models to be efficiently solved. The discretization is performed using four-point orthogonal Radau collocations on finite elements in the time domain and backward finite differences in the axial domain. Collocations were chosen for the time domain because of their accuracy and built-in functionality within Pyomo. To achieve an accurate dynamic model, this discretization was prioritized such that the time interval $\Delta t = 12.5\ s$ (i.e., 8 intervals in a 100 second time horizon) was chosen as the finite element size in both absorber and tank models. A more parsimonious $n_{fez} = 10$ finite elements were used in the absorber axial domain to keep the model size as small as possible without sacrificing accuracy in the solution.

Table 5: Inputs required by the absorber section model

	Initial conditions $(\mathbf{0} \le \boldsymbol{z} \le \boldsymbol{H}, \boldsymbol{t} = \mathbf{0})$	***Boundary conditions*** $(\boldsymbol{z} = \mathbf{0}, \boldsymbol{z} = \boldsymbol{H}, \boldsymbol{t} \ge \mathbf{0})$
Absorber (gas)	$C_i^g(z,0) = C_{i,0}^g(z)$	$C_i^g(0,t) = C_{i,in}^g(t)$
	$T_g(z,0) = T_{g,0}(z)$	$T_g(0,t) = T_{g,in}(t)$
		$u^g(0,t) = u_{in}^g(t)$
Absorber (liquid)	$C_i^l(z,0) = C_{i,0}^l(z)$	$C_i^l(H,t) = C_{i,in}^l(t)$
	$T_l(z,0) = T_{l,0}(z)$	$T_l(H,t) = T_{l,in}(t)$
		$u^l(z,t) = u_{in}^l(t)$
Tank	$T^{tank}(0) = T_0^{tank}$	
	$h(0) = h_0$	

	$n_i(0) = n_{i,0}$	

Prior to discretization, the models (i.e., absorber and tank) have a collective 16 states and 210 algebraic variables, which grows to 116 states and 1,977 algebraic variables with absorber axial discretization (i.e., when solving the RTO problem). This further grows to 3,712 states and 63,168 algebraic variables with axial discretization of the absorber and time discretization of the entire absorber section (i.e., when solving the NMPC and MHE problems). The states of the system are the differential variables in the previously presented differential equations (i.e., the liquid and gas concentrations and temperatures in the absorber as well as the molar holdups, liquid level, and temperature in the tank). The algebraic variables correspond to all other phenomenological and physical property models in the system. An interior-point algorithm [46] was used to solve the large-scale optimization problems described in the following sections on an Intel core i7-4770 CPU @ 3.4 GHz. Both steady-state and dynamic versions of the models described in this equations (4)–(13), Table 2, Table 3, and equations (15)–(17) (in the steady-state case) are used in the proposed scheme. The collective vector of equations representing the discretized models is denoted as $\boldsymbol{f_s}$ in its steady-state version and $\boldsymbol{f_d}$ its dynamic version.

In addition to the initial and boundary conditions, the PCC absorber section case study considered herein also requires additional inputs in the form of the manipulated variables and the disturbance variables. In the PCC absorber section, the manipulated variables which act as control actions are the flowrate of solvent solution into the absorber, the fresh MEA makeup flowrate into the tank, the fresh water makeup flowrate into the tank, and the tank cooling duty; i.e., $\boldsymbol{u} = [F_{l,in}^{abs} \quad F_{MEA}^{mkup} \quad F_{water}^{mkup} \quad Q_{cool}]^{\mathbf{T}}$ as depicted in Figure 3. Manipulation of both makeup streams is a key novelty within this work as they can significantly impact the economics and operation of the absorber section of this plant. For this purpose, a centralized MPC approach is best suited as it can model and account for the interaction between the makeup streams, the amount of carbon captured, and the tank level.

The operation of an actual PCC system is subjected to disturbances that can have significant effects on the process behaviour and economics. In this study, the main disturbances being considered are: 1) the flue gas flowrate, which varies based on the load variation in the upstream power plant; 2) the flue gas CO_2 content, which varies based on the fuels being used in the upstream power plant; and 3) the recycle stream flowrates, which vary based on the makeup fed to the system and the operation of the stripper section reboiler. Changes in the flue gas CO_2 content are assumed to be reflected by changes in the flue gas water content (i.e., a 0.01 fraction increase in CO_2 is accompanied by a 0.01 fraction decrease in H_2O in the flue gas); hence, changes in the fractions are treated as a single disturbance variable. Accordingly, the disturbances considered in this work are denoted as $\boldsymbol{d} = [F_g^{flue} \quad y_{CO_2}^{flue} \quad F_{MEA}^{rec} \quad F_{CO_2}^{rec} \quad F_{H_2O}^{rec}]^{\mathbf{T}}$; these are depicted in Figure 3.

In the PCC absorber section, the controlled variables comprise the percent carbon capture ($\%CC$), the MEA concentration in the lean solvent ($C_{MEA}^{tank}(mol/L)$) from buffer tank to absorber, the buffer tank temperature ($T^{tank}(K)$), and the buffer tank level ($h^{tank}(m)$); i.e., $\boldsymbol{Y} = [\%CC \quad C_{MEA}^{tank} \quad T^{tank} \quad h^{tank}]^{\mathbf{T}}$. The percent carbon capture is defined as follows:

$$\%CC = \frac{F_g^{flue} y_{CO_2}^{flue} - F_g^{vent} y_{CO_2}^{vent}}{F_g^{flue} y_{CO_2}^{flue}} \times 100\% \tag{18}$$

where $F_g^{in}(mol/s)$ and y_{CO_2} are the flue gas flowrate and CO_2 fraction, respectively. $F_{CO_2}^{vent}$ (mol/s) is the CO_2 flowrate in the vent gas.

This nominal operation occurs at the nominal values for the manipulated variables $\boldsymbol{u_{nom}} = [32.17 \quad 0.0002 \quad 0.2 \quad 139{,}000]^{\mathbf{T}}$ and the nominal values for the disturbances $\boldsymbol{d_{nom}} = [4.012 \quad 0.175 \quad 3.2098 \quad 0.98 \quad 27.78]^{\mathbf{T}}$; these correspond to the nominal controlled variables $\boldsymbol{Y_{nom}} = [96.23 \quad 4847 \quad 314 \quad 1]^{\mathbf{T}}$ [38,39,47]. The complete stream data for the nominal conditions as predicted by the current model can be found in Table B1 (Appendix B). Combinations of nominal disturbance variables and nominal manipulated variables are used as the initial or final operating conditions for several of the operational cases presented in section 5.

3.6. Model validation

The model presented in the previous section was validated using different sources of data available in the literature as a single set of comprehensive data for this system is unavailable. Table 6 presents a comparison of outlet stream predictions for the nominal operation (i.e., corresponding to $\boldsymbol{u_{nom}}$, $\boldsymbol{d_{nom}}$, and $\boldsymbol{Y_{nom}}$) of the absorber model as implemented in this study and of a previous mechanistic model reported in the literature [39]. The authors of the prior model provided detailed data on the outlet streams at the nominal operating condition defined previously and in Table B1 (Appendix B); this included compositions, flowrates, and temperatures; these can be compared to predictions of the present model.

Table 6: Comparison of absorber output predictions against previously reported mechanistic model implementation. Error of predictions of present study with respect to [39] also presented.

	Vent gas		**Rich solvent**	
	Present study	**Harun et al. [39]**	**Present study**	**Harun et al. [39]**
Temperature (K)	314.06	314.15	319.89	327.76
Flowrate (mol/s)				
MEA	0.0000	0.0000	3.2098	3.3560
CO_2	0.0427	0.0295	1.6393	1.6534
Water	0.2340	0.2259	27.8460	27.8573
N_2	3.2100	3.2146	0.0000	0.0000
Total	3.4867	3.4700	32.6951	32.87
Mean error (%)		8.1641		1.3638

As shown in Table 6, the predictions made by the current model conform well with previous model predictions (mean output predictions < 8.2 % error). In particular, the error of the vent gas stream is elevated by the CO_2 composition; nevertheless, this composition is very small in magnitude ($\sim 1\ mol\%$) so small inaccuracies tend to inflate the error. This suggests that the absorber column boundaries (i.e., outlets) are being predicted well without making conclusions as to the accuracy along the absorber height. While having validation at the nominal operation is acceptable, a complete validation at various operating conditions is necessary to conclude that the model is valid for a range of operations. Two key process variables for which there is experimental as well as simulated data across several operating conditions are the solvent temperature and the $\%CC$. By analyzing solvent temperature profiles, the

existence of the so-called temperature bulge, which is characteristic of the reactive mechanism in the PCC absorber, can be verified. Moreover, the conformance of the absorber predictions can be assessed. Although a set of experimental data of compositions along the absorber height is not available due to the intractability of online composition analysis for this system, the $\%CC$ can be obtained from the boundary compositions and has been reported. By analyzing the $\%CC$, it can be verified that this key performance variable is indeed being predicted accurately; this is particularly important in the RTO and NMPC layers where the $\%CC$ is being used explicitly to define set points. [42] presents two experimental data sets (temperature profiles and corresponding $\%CC$) and an additional two simulated temperature profiles (generated by their own model). The former are named case 1 and 2 in the present study while the latter simulated profiles are referred to as case 3 and 4 in the present study. The temperature profiles that comprise cases 3 and 4 were sampled at regular intervals to generate individual data points. Each case represents a significant change in operating conditions via the flue gas flowrate, composition, and temperature; the lean solvent flowrate, composition, and temperature; as well as the column packing height. The inlet compositions required to achieve these profiles along with their naming conventions in [42] can be found in Appendix B, Table B2. Figure 4 shows the temperature profiles predicted by the present model along with data for temperatures from [42] for the four different operational cases while Table 7 presents the error in the predictions made by the model in the present study with respect to the data from [42].

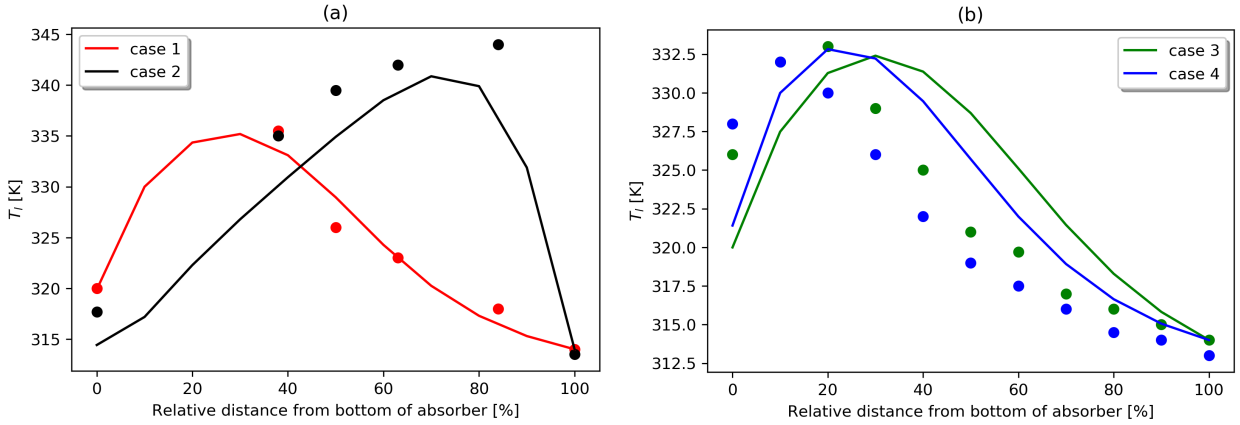

Figure 4: Temperature profile prediction for various operating cases. a) experimental data, b) simulated data.

Table 7: Comparison of absorber temperature profiles and %CC predictions against previously reported data. Error of predictions of present study with respect to [42] also presented.

Case #	**$\%CC$ present study**	**$\%CC$ [42]**	**Error in $\%CC$ (%)**	**Mean error in T_l (%)**
1	95.03	93.85	1.257	0.310
2	72.07	70.95	1.578	3.781
3	86.77	86.20	0.661	2.700
4	93.61	93.35	0.278	2.892

As shown in Figure 4, the temperature profiles align closely with the data from [42], this is corroborated by the low mean errors in T_l presented in Table 7 ($< 4\%$ across all operating conditions). The present model slightly underestimates the profiles for the entire length of the column in case 2 while, in cases 3 and 4, the present model

underestimates the profiles prior to the bulge and overestimates after the bulge. Moreover, they key $\%CC$ predictions made by the present model conform with the data from [42] even more closely ($< 2\%$ across all operation conditions). This close agreement in temperature and $\%CC$ predictions compared to [42] are well within the range of acceptability for the wide range of operating conditions summarized in Table B2. Moreover, the accuracy of outlet stream predictions compared to [39] summarized in Table 6 given further confidence in the accuracy of the model as it is an independent data set. These findings suggest that the current absorber model conforms with past models as well as experimental data, thus it is adequate for use in the present study. Additionally, the simplified reboiler correlation in section 3.4 was also shown to accurately correlate reboiler duty to lean loading (which serves as an input to the absorber as show in Table B2) within the range being considered in this study with $R^2 = 0.97$, implying small residuals and highly correlated data.

4. Scheme implementation and assessment

The specifics of the implementation of the model presented in section 3 to the scheme proposed in section 2 are presented next along with the assessment tools used for different layers within the scheme.

4.1. RTO implementation and assessment

The RTO uses the economic function presented in equation (1) along with a steady-state version of the mechanistic process model and stripper approximations described in section 3.4 to determine the economically optimal steady state for the controlled variables. State measurements are typically fed to the RTO such that a parameter estimation problem is solved prior to the economic optimization procedure. In this study, we assume no parametric mismatch, thus not requiring the parameter estimation step. However, the steady-state wait-time associated with the parameter estimation step is enforced using the following heuristic for triggering of the RTO:

$$\boldsymbol{Y_t - Y_{t-i} < 0.005 Y_{nom}} \qquad \forall i \in \{1, \dots, 10\} \quad (19)$$

which declares that the system is at steady state when the controlled variables are changing at a rate of less than 0.5% of their nominal value from the current sampling interval to the previous ten sampling intervals. A simple heuristic such as this is assumed to be acceptable for the present PCC case study; for more sophisticated methods, the field of steady-state detection provides ways to automate this trigger [36].

The additional correlations (15)–(17) are included within the steady-state model $\boldsymbol{f_s}$ such that decisions can made regarding the reboiler operation without explicitly considering it in the control scheme. With the inclusion of the stripper section approximations within $\boldsymbol{f_s}$, the RTO objective function in equation (1) as it pertains to the system described in section 3 simplifies to:

$$C_{process} = P_{MEA}\dot{m}_{MEA}^{mkup} + P_{sales}(\dot{m}_{CO_2,in}^{g} - \dot{m}_{CO_2,out}^{g}) + P_{CO_2}\dot{m}_{CO_2,out}^{g} + P_{steam}Q_{reb} \quad (20)$$

where $C_{process}(\$CAD/s)$ is the cost of operating the PCC absorber section. $\dot{m}_{MEA}^{makeup}(tn/s)$ is the flowrate of fresh makeup MEA into the system as shown in Figure 3; this is the only chemical cost considered in this case. $\dot{m}_{CO_2}^{cap} = \dot{m}_{CO_2,in}^{g} - \dot{m}_{CO_2,out}^{g}(tn/s)$ and $\dot{m}_{CO_2,out}^{g}(tn/s)$ are the flowrate of carbon captured and emitted, respectively, by the absorber. $Q_{reb}(W)$ is the reboiler duty as modelled by steady-state lean loading equation (14), which is an additional decision variable aside from the controlled variables; this is the only energy cost considered in this case. In this case

study, the efficiency factor introduced in equation (1) was assumed to be $\zeta = 1$ for simplicity. Moreover, pumping and water costs are assumed to be negligible.

Another consideration when optimizing the PCC plant is the impact it has on the upstream power plant. Namely, operating the PCC plant with higher reboiler duty decreases the power plant profits by using steam that could otherwise be used for power generation. To analyze the impact, the lost profits owed to reboiler operation were estimated as:

$$C_{energy} = \Delta Q_{reb}(P_{elec} - P_{steam})\eta \tag{21}$$

where $C_{energy}(\$CAD/yr)$ are the lost profits (energy penalty) owing to reduced energy generation, $\Delta Q_{reb}(MW)$ denotes the difference between the current reboiler duty and its previous or nominal value, P_{elec} is the price of electricity sold to consumers. The efficiency factor (η) accounts for the losses in converting thermal energy from combustion-generated steam to electrical energy for consumers. For the present absorber section case-study, this factor is defined as $\eta = 0.4$ [48]; however, this user-defined parameter may vary depending on the power plant. The price term uses the difference between the electrical sales cost and the steam cost to evaluate the losses not already considered within $C_{process}$; in this way, only sales cost mark-up is considered (i.e., the raw steam cost is not double counted). This additional energy penalty to the power plant can be compared against the savings achieved by the PCC RTO to have a more complete perspective on the economic impact. The prices associated with equations (20) and (21) are summarized in Table 8.

Table 8: Prices for economic terms, adjusted for inflation and converted to $CAD.

Term	**Value**	**Source**
MEA (P_{MEA})	2420 $\$CAD/tn\ fresh\ MEA$	[49]
Sales (P_{sales})	-50 $\$CAD/tn\ CO_2\ sold$	[35]
CO_2 (P_{CO_2})	176 $\$CAD/tn\ CO_2\ removed$	[50]
Steam (P_{steam})	0.065 $\$CAD/kWh$	[51]
Electricity (P_{elec})	0.115 $\$CAD/kWh$	[52]

There is little consensus on the true SCC, and various models have been proposed in the literature [50]. In this work, we estimated the price using the DICE-2016R with a 2.5% discount rate. Note that this is the first time this cost is used in the economic optimization of a PCC process.

The lower and upper bounds for the controlled variables ($\boldsymbol{Y^l}$ and $\boldsymbol{Y^h}$) are set as follows:

$$0 \leq \%CC \leq 100 \tag{22}$$

$$3000 \leq C_{MEA}^{tank}\ (mol/L) \leq 6000 \tag{23}$$

$$300 \leq T^{tank}\ (K) \leq 345 \tag{24}$$

$$0.05h^{tank} \leq h\ (m) \leq 1.95h^{tank} \tag{25}$$

The constraint on the controlled variable for the tank level is an important safety constraint to avoid overflowing and imposes that the tank level's set point does not exceed the physical tank dimensions (within a 5% safety factor).

Moreover, the tank temperature constraint ensures that the absorber feed temperature is within an acceptable range for this operation.

Using the new economic function described in equation (1) and their adaption for this case study in equation (20), the RTO passes updated controlled variables as set points (i.e., $\boldsymbol{Y_{sp}} = \boldsymbol{Y}$) to the NMPC upon its execution which, as mentioned, requires for the controlled variables to be steady in time by the criteria described in equation (19).

In addition to the set point update, the execution of the RTO also incites a ramp disturbance in the recycle flowrates through the approximated model described in section 3.4. In other words, the recycled flowrates ramp from their outdated values to those specified by the RTO. A ramp is used such that there is a delay between making stripper side decisions and their effect on the absorber as these changes would not occur instantaneously in the plant. As mentioned in section 3.5, the recycled stream is treated as a disturbance for the NMPC to reject when the set points are changed. The treatment as a disturbance is necessary as the NMPC does not have a stripper section model to predict the behaviour of the recycle stream. The ramp begins when the RTO is executed and last for 200 time intervals (i.e.~40 minutes), when the recycle stream reaches its new flowrate and composition as specified by the RTO. This number of sampling intervals (~40 minutes) was chosen to model the time-delay between changes on the absorber/stripper sections and their effect on the recycled stream (i.e. changes in makeup streams and heat duty will not have immediate effects on the recycle stream). A similar delay was observed in open-loop tests by [38], thus supporting the assumption that stripper section dynamics would occur gradually.

For the overall integrated scheme, the performance is economically driven, thus the process economics are assessed through an annualized version of the RTO objective function in equation (20) at every sampling interval. Additionally, the payback period $t_{payback}(h)$ is used to quantify the amount of time that the process must be operated at a new steady state for to justify the execution of the RTO. This term is defined as follows:

$$t_{payback} = \tau_{annum} \frac{\int_{t_0^{RTO}}^{t_f^{RTO}} C_{PCC} dt}{C_{PCC}^0 - C_{PCC}^f} \tag{26}$$

where t_0^{RTO} and $t_f^{RTO}(hr)$ denote the initial and final times at which a given RTO execution imposes dynamic operation on the plant, respectively (i.e., t_0^{RTO} is the time at which the RTO is executed and t_f^{RTO} is the time at which the set point change is completed). C_{PCC}^0 and $C_{PCC}^f(\$CAD/yr)$ denote the initial (unoptimized) and the final (optimized) steady-state cost of the plant operation. τ_{annum} $(8760\ hr/yr)$ is used to convert the annualized costs to payback periods in hours.

4.2. NMPC implementation and assessment

In the proposed NMPC controller, the horizons are set to be equivalent and equal to 100 seconds (i.e., $P = C = 100s$), these were previously found to provide good control performance [21]. The first term in the objective function in problem (2) is weighted using the diagonal matrix $\boldsymbol{Q_c} = diag(4,2,3 \times 10^4, 5 \times 10^{-4})$, which aims to regulate the system towards its set points. The second term in the objective function is weighted by the diagonal matrix $\boldsymbol{R_c} = diag(3.5 \times 10^7, 2 \times 10^3, 30, 2 \times 10^{-8})$, which supresses sudden changes in the manipulated variables. The dynamic performance of the proposed scheme is dependent on these tuning parameters as they balance tracking speed with aggressive changes in the manipulated variables. These must be balanced as fast tracking is desired for good

performance, but overly quick control actions put undue burden on process equipment (i.e., manipulated variables). For this case study, preliminary closed-loop simulations as well as RGA analysis were used to tune the controller weights. The former helped in tuning the move-suppression matrix to ensure unrealistically fast control actions were supressed, while the latter served as a guideline to assess interactions between variables such that high interaction was avoided while evenly prioritizing the control objectives. This unique tuning and structure of the controller makes it difficult to compare to previous control approaches, which have different control mechanisms and priorities.

As with the RTO, $\boldsymbol{Y^l}$ and $\boldsymbol{Y^h}$ are the lower and upper bounds for the controller variables, respectively, as outlined in equations (22)–(25), and $\boldsymbol{u^l}$ and $\boldsymbol{u^h}$are the lower and upper bounds for the manipulated variables, respectively. The manipulated variable bounds are defined as follows:

$$0 \leq F_{l,in}^{abs}\ (mol/s) \leq 100 \tag{27}$$

$$0 \leq F_{MEA}^{mkup}\ (mol/s) \leq 5 \tag{28}$$

$$0 \leq F_{water}^{mkup}\ (mol/s) \leq 2 \tag{29}$$

$$-500{,}000 \leq Q_{cool}\ (W) \leq 0 \tag{30}$$

These bounds are chosen such that they provide the manipulated variables with a realistic range, while still providing operational flexibility. Note that the cooling duty in equation (30) is negative as heating is positive in the convention used herein. Using this NMPC tuning, horizon, and bounds, the economically important controlled variables (i.e., carbon capture and MEA content going to the absorber) can be tracked quickly and flexibly using makeup streams while also considering safety limitations (i.e., in the tank level and temperature).

Assessment of the control scheme is performed by analyzing the transient times and shape of the responses observed in the system. Moreover, the sum of squared errors (SSE) between each controlled variable and its respective set point is computed as follows:

$$\boldsymbol{SSE} = \sum_{i=1}^{n} \left(\boldsymbol{Y_i} - \boldsymbol{Y_{i,sp}}\right)^2 \tag{31}$$

where n is the number of sampling intervals un a given scenario and $\boldsymbol{SSE} \in \mathbb{R}^{n_Y}$ denotes the vector of SSE for the controlled variables. The tracking performance of each variable is assessed separately as they have largely different magnitudes and controller tunings, thus prohibiting their direct comparison. Using SSE, the performance of the controller is quantified through its tracking performance.

4.3. MHE implementation and assessment

In the present work, the MHE is formulated such that only a few realistically achievable measurements are required for state estimation; this is enabled by the mechanistic MHE model. This is the first MHE implementations for any PCC plant that uses a mechanistic model, few measurements, and does not require decomposition of the column axial domain into subdomains with their own estimators.

The discretization necessary to solve the axially distributed absorber model poses a measurability challenge because each of the n_{fez} discretization point along height domain requires an initial condition to solve the NMPC problem. For instance, online measurement of the concentrations along the column height is not practical because analysis of stream compositions is time and resource intensive. Accordingly, only the inlet stream (boundary) compositions into

the absorber are assumed to be measurable; this leaves the compositions along the $n_{fez} - 2$ remaining column heigh discretization points to be estimated. Conversely, the temperatures at every spatial discretization point in the column are assumed to be measurable. Having several temperature measurements is realistic since only conventional thermocouples are only required. Furthermore, the states in the storage tank are comparatively fewer as they only include the level, temperature, and molar holdup. The temperature measurement in the tank is realistic as it only requires a thermocouple, while measuring level is also commonplace using pressure transmitters/transducers. In total, 32/116 system states are assumed to be measured online and are as follows:

$$\boldsymbol{z_t} = [\boldsymbol{T_l^{abs^T}} \quad \boldsymbol{C_{n_{fez}}^{l,abs^T}} \quad \boldsymbol{T_g^{abs^T}} \quad \boldsymbol{C_0^{g,abs^T}} \quad T_l^{tank} \quad h_l^{tank}]^{\mathbf{T}} \tag{32}$$

where $\boldsymbol{T_l^{abs}}$ and $\boldsymbol{T_g^{abs}} \in \mathbb{R}^{n_{fez}}$ denote the liquid and gas temperature measurements along the absorber column height, respectively. $\boldsymbol{C_{n_{fez}}^{l,abs}}$ and $\boldsymbol{C_0^{g,abs}} \in \mathbb{R}^{n_{comp}}$ denote the liquid and composition measurements at the absorber column boundaries, respectively. T_l^{tank} and $h_l^{tank} \in \mathbb{R}$ denote the tank temperature and level measurements, respectively.

The molar holdup in the tank is readily observable as it is assumed that the composition of inlet from tank to absorber is measurable; thus, the concentration of the tank is also known due to the well-mixed assumption. This is estimated as follows:

$$\boldsymbol{n^{tank}} = \pi(D^{tank}/2)^2 h_l^{tank} \boldsymbol{C_{n_{fez}}^{l,abs}} \tag{33}$$

where $\boldsymbol{n^{tank}} \in \mathbb{R}^{n_{comp}}$ denotes the molar holdup in the tank. In the present PCC absorber section case study, as some of the states are directly measured and some can be calculated, $\boldsymbol{h_d}$ is effectively a diagonal matrix of proper dimensions augmented with the tank holdup equation (33) (i.e., $\boldsymbol{h_d} \in \mathbb{R}^{(N_z+n_{comp})\times N_z}$).

The MHE horizon used in this study was set to be of the same length as the NMPC horizons (i.e., $N = P = C = 100s$). This horizon was determined through preliminary closed-loop tests and was found to be long enough to achieve a good state estimate without the approximation of an arrival cost that is often required in MHE problems [37]. A shorter horizon resulting in a more parsimonious MHE problem would be enabled by the inclusion of arrival cost; however, this is out of the scope of the present study.

In the present scheme, the measured/calculated buffer tank states are passed directly to the NMPC while the estimated absorber states must be solved for by the MHE and then passed to the NMPC. Since the tank measurement are noisy as they do not experience the filtering effects of the MHE, a first-order filter with a constant of $\lambda = 0.5$ is imposed on the states of the tank provided to the NMPC to mitigate the noise effects in the control actions, i.e.:

$$\begin{aligned} T_{l,t}^{tank,F} &= \lambda T_{l,t-1}^{tank,F} + (1-\lambda) T_{l,t}^{tank,m} \\ h_{l,t}^{tank,F} &= \lambda h_{l,t-1}^{tank,F} + (1-\lambda) h_{l,t}^{tank,m} \\ \boldsymbol{n_t^{tank,F}} &= \lambda \boldsymbol{n_{t-1}^{tank,F}} + (1-\lambda) \boldsymbol{n_t^{tank,m}} \end{aligned} \tag{34}$$

where superscripts F and m denote a filtered and a measured value, respectively.

Using the observation strategy and horizon outlined, the scheme can provide accurate state estimates for the NMPC to produce effective control actions. The quality of these estimates is assessed by analyzing the mean squared error (MSE) between the estimated and true $\%CC$. MSE is defined as follows:

$$MSE = \frac{1}{n}\sum_{i=1}^{n}\left(\%CC_{i,T} - \%CC_{i,e}\right)^2 \quad (35)$$

where n is the number of sampling intervals in a given scenario (or for a given time span) and the subscripts T and e denote the true and estimated $\%CC$ for sample i, respectively. The MSE of $\%CC$ is used as a proxy to assess the performance of the MHE as only the absorber states are estimated and $\%CC$ is the most crucial output from the absorber portion of the model.

5. Results and discussion

To evaluate the performance of a real-life PCC plant, the proposed closed-loop scheme shown in Figure 1 was implemented in the pilot-scale system described in the previous section. The transient operation of the system is described using the dynamic model $\boldsymbol{f_d}$, where noise is added to the process and the measurements. Process noise (i.e., owed to unmodelled fluctuations in the system) is inserted via the initial conditions between one simulation interval and the next, while measurement noise (i.e., owed to instrumentation errors) is inserted via the measured states passed to the MHE. Both of these noises are assumed to be zero mean, normally distributed, with a standard deviation of 0.02% of the corresponding nominal state values, i.e. $\mathcal{N}(0, (0.0002\boldsymbol{x_{nom}})^2)$ where $\boldsymbol{x_{nom}}$ is the state vector corresponding to the nominal operation indicated in Table B1.

As noted in section 3.3, the model parameters used herein are experimentally determined from prior studies. Accordingly, the present work assumes that they manifest at their nominal value in both the plant and the mechanistic models used in the proposed scheme (i.e., no structural or parametric mismatch was assumed). However, if parametric uncertainty were observed, the scheme would experience some deterioration owing to a loss in control, estimation, and RTO performance.

5.1. Scenario A: cofiring of fuels

Cofiring refers to the operation of a power plant that combusts different types of fuels within the same operating period to lessen the environmental impact of a highly emissive fuel. One such emissive fuel is coal and, as there is a greater shift to renewables, the potential of cofiring with biomass [53] is being increasingly investigated in terms of feasibility and benefits. However, this operational case (co-firing) has yet to be examined through an economic optimization framework, which can help to further reduce emissions as well as cost.

In this scenario, the cofiring of biomass and coal is illustrated through its impact on the flue gas composition being supplied by the power plant to the downstream PCC absorber section. The scheme presented in this work is particularly well-suited for this scenario as the RTO can find new economically optimal steady states depending on the fuel used in the combustion process. In this scenario, only the transition between 100% biomass and 100% coal firing is studied; however, the proposed RTO framework for this case study is suited to determine set points for any fuel ratio in between. The starting point for this scenario corresponds to the nominal manipulated variables values presented in section 3.5 and the PCC plant operating downstream from a biomass-fired plant ($y_{CO_2} = 0.12$). From this initial operation, coal ($y_{CO_2} = 0.175$) is introduced into the upstream power plant with the fuel ramping up from 0% coal content to 100% coal content within a span of 200-time intervals (~40 minutes). This is reflected in a flue gas CO_2 fraction that ramps from 0.12 (fully biomass-fired) to 0.175 (fully coal-fired), as shown in Figure 5a. The controller first rejects the disturbance imposed on the flue gas composition by the change in fuel, reaching a new steady state at

~7.5 hours as determined by meeting the criteria in equation (19). At this time, the RTO is executed such that an economically optimal set point is found for the new flue gas composition corresponding to coal-firing.

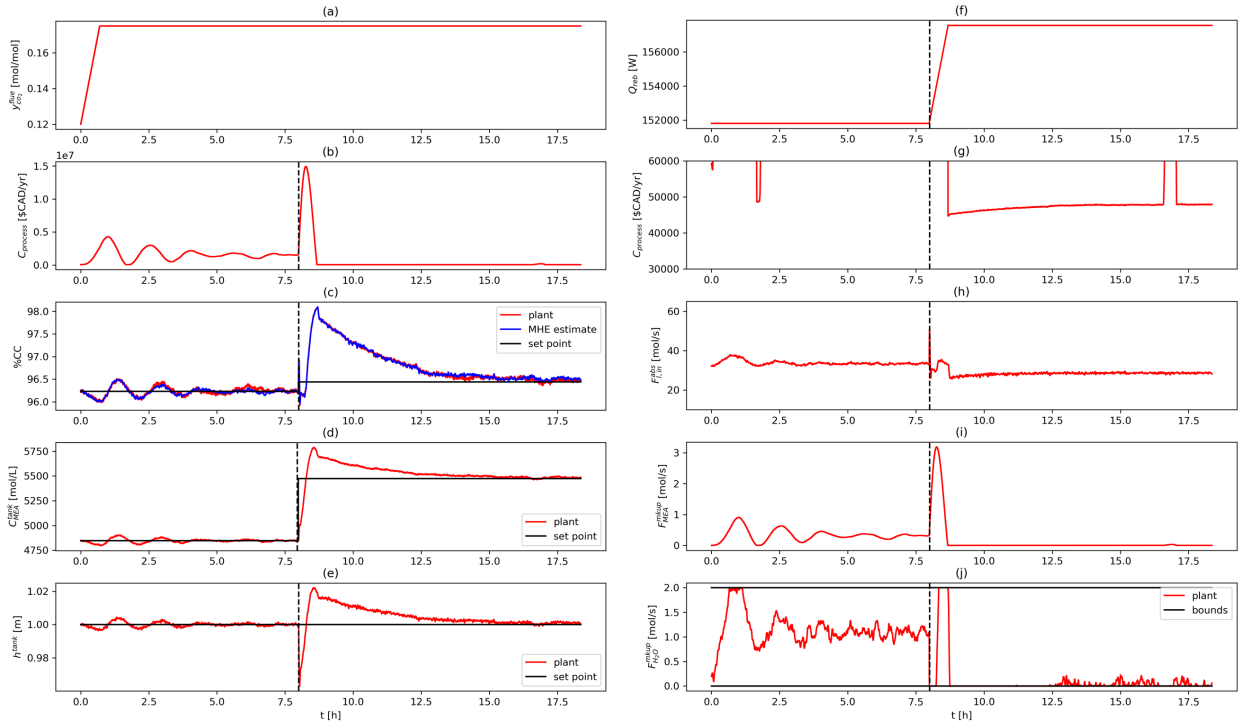

Figure 5: Flue gas CO_2 content, process cost (b shows full profile, g shows zoomed in profile), controlled variables, and manipulated variables for a cofiring scenario. Dashed vertical lines represent times at which the RTO was executed, thus inciting a set point change.

The responses on the buffer tank temperature and cooling duty in this scenario can be found in Figure A3 (Appendix A). In general, the temperature is tracked quickly and has little impact on the process economics. Contrastingly, the other controlled variables (i.e., $\%CC$, C_{MEA}^{tank}, and h^{tank}; Figure 5c, 5d, 5e, respectively) are tracked more slowly. This occurs as the tank inlet and outlet flowrates, which affect the level, interact with the removal rate and MEA concentration; thus, a slower coordinated response is made by the NMPC to track these interacting controlled variables.

Figure 5c shows the plant $\%CC$ along with the MHE-estimated $\%CC$; for this scenario, the MHE estimates were observed to be in good agreement with the true plant with an $MSE = 1.239 \times 10^{-3}$. This is the case for all scenarios in the present study and is owed to the use of the mechanistic model in this layer and the use of a long horizon in the MHE framework. Nevertheless, the MHE occasionally drifts from the true states as can be seen during some time periods in Figure 5c (i.e., $t \cong 6\,h \rightarrow 6.9\,h$ with $MSE = 6.830 \times 10^{-2}$ and $t \cong 13.7\,h \rightarrow 14.4\,h$ with $MSE = 5.160 \times 10^{-2}$).

To gain further insight into the effect of the proposed RTO framework, a 'no-MHE' case was performed whereby the cofiring scenario is repeated with the assumption of full access to the system states. This occurs when all the true plant states can be measured thus making the state estimation framework (i.e., MHE) unnecessary. In principle such a 'no-MHE' case is unrealistic as composition measurements are difficult to perform online for the PCC absorber;

nevertheless, it is valuable to assess the performance of the proposed scheme under this assumption to assess the impact and need of a reliable estimation scheme. Note that previous economic operation studies in PCC have not considered an estimation scheme and hence have not addressed the issue of state accessibility. Since the MHE provides state estimates to the NMPC, which may differ from the true plant states, the controller and economic performance can be affected by using estimation. Hence, the 'no-MHE' case enables observation of the deterioration that an estimation scheme causes on the operational framework. For the present 'no-MHE' case, the first-order filter with $\lambda = 0.5$ is imposed on all states to smooth noise and the RTO is assumed to be executed at the same time as the MHE scenario. As the SSE described in equation (31) quantifies the tracking performance of the NMPC, this measure can be used to assess the controller performance under the MHE and 'no-MHE' cases. To make a fair comparison, the NMPC controller tuning parameters, and characteristics remain the same for both scenarios. Table 9 summarizes the tracking performance under the MHE and 'no-MHE' scenarios.

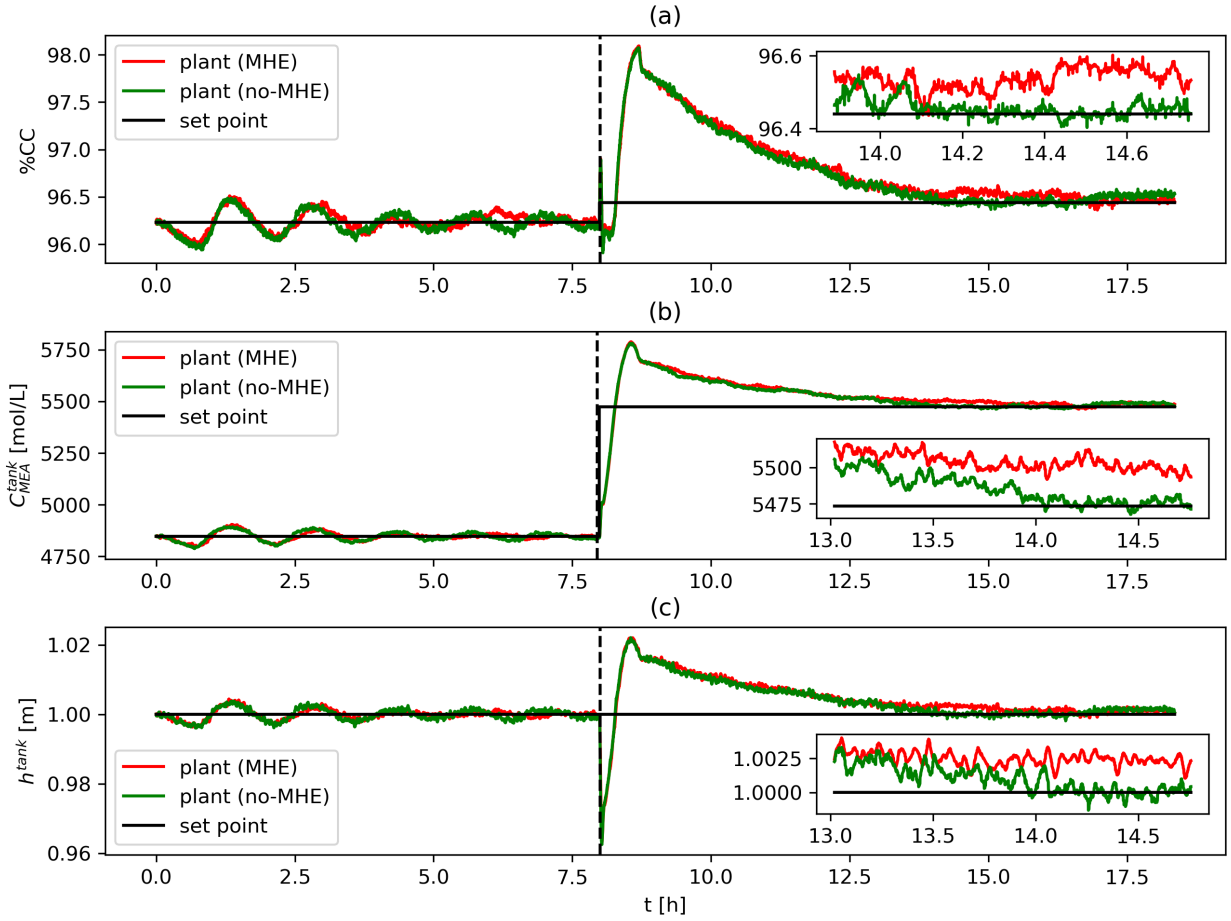

Figure 6: Controlled variables in MHE and no-MHE cases for Scenario A. Sub-windows display ranges in which MHE-induced performance loss is most severe.

Table 9: Effect of MHE on control and economic performance for Scenario A.

Controlled variable	***SSE*** **(MHE)**	***SSE*** **(no-MHE)**	**Performance loss** (%)

$\%CC$ (%)	3827	3657	4.649
C_{MEA}^{tank} (mol/L)	1.530×10^8	1.416×10^8	8.051
T^{tank} (K)	30.68	23.56	30.22
$h^{tank}(m)$	0.7931	0.7376	7.524
Economics	**Cost (MHE)**	**Cost (no-MHE)**	
$\int_0^{18h} C_{process} dt$ $(\$CAD)$	9018	8977	0.4567

As displayed in Table 9 and the drift observed in the controlled variable plots (Figure 6a, 6b, 6c, particularly the sub-windows), the tracking performance is better in all 'no-MHE' controlled variables as reflected by lower SSE values in Table 9. The 'no-MHE' case provides an upper bound for controller performance as it has access to the true plant states and, in principle, the control performance is best when true plant states can be measured. In contrast, the MHE estimates were shown to sometimes drift from the actual plant states, thus adversely affecting performance. As such, the percent error of the MHE case with respect to the 'no-MHE' case reflects the loss in controller performance owed to the MHE. Nevertheless, the MHE case reflects a more realistic condition since most of plant states are often not available for online control. These losses due to the MHE estimation are generally low ($< \sim 8\%$) except for that of the tank temperature; however, the temperature dynamics are fast compared to other controlled variables and the deviations from the set points are primarily due to noise as shown in Figure A3 (Appendix A). The speed of the tank temperature dynamics, and the fact that there is little deviation from its set point in both MHE and 'no-MHE' cases (SSE is on the order of 20–30 across the entire simulation while the nominal tank temperature is on the order of $314\ K$) suggest that the deterioration in tank temperature tracking performance caused by the MHE is negligible in reality because the deviations are caused by noise, thus this variables will not have a significant impact on the rest of the process. In terms of economics, there is little difference in the total process cost as reflected by the cost integral in Table 9 whereby the economic loss of the MHE case with respect to the 'no-MHE' case is low. This implies that the loss in tracking performance caused by the MHE does not propagate to the economics because the economic improvements are being achieved in the steady-state phase. That is, the MHE was able to track the true plant states accurately using only a low number of measurements available in the plant. While at steady state, the behaviour of the controlled variables in the MHE and 'no-MHE' cases in Figure 6 are observed to have essentially no offset (hence no economic loss). Additionally, Figure 5c displays the true $\%CC$ and the MHE-estimated $\%CC$, which again show virtually no offset while at steady state. These results highlight the benefits in using an advanced state estimation scheme such as MHE for the optimal operation of PCC plants. We can conclude that the deterioration from a control and economic perspective caused by the MHE is acceptable considering how few measurements are used and the level of noise. Thus, the MHE performs well in estimating the system states and its application is not a significant detriment on the larger scheme. This result is of prime importance since state estimation will always be necessary for plants such as the PCC system since many plant states cannot be measured online.

As shown in Figure 5c, 5d, and 5e, following the ramp disturbance at $t = 0\ h$, the NMPC was able to track the system back to its original set points by $t \cong 7.5\ h$ with a few damped oscillations. The initial ramping in the flue gas content

from 0 to $t \cong 0.7\ h$ hours cause the flowrate manipulated variables (i.e., Figure 5h, 5i, and 5j) to also ramp to minimize the effect of the disturbance on the controlled variables. Once the ramp has been completed, hysteresis from this initial ramping action causes the NMPC to modulate the manipulated variables to quickly track the set points. A less aggressive controller tuning (i.e., more weight on control move suppression terms) could have resulted in less oscillation at the expense of control speed; however, due to the stable nature of the PCC system these small oscillations are deemed acceptable.

The increase in CO_2 content in flue gas initially disturbs the system such that the original $\%CC$ cannot be maintained with the pre-disturbance MEA content in the solvent fed to the absorber; thus, rejecting the disturbance to the $\%CC$ is achieved through the increase of the MEA makeup flowrate, as shown in Figure 5i. While the initial makeup flowrate is merely $0.0002\ mol/s$, the flowrate after the disturbance rejection is $\sim 0.4\ mol/s$, thus constituting a two thousandfold increase in the flowrate. Despite the relatively low unit price of MEA, the disturbance rejection phase of the scenario leads the process to a very economically disadvantageous combination of controlled and manipulated variables as the high MEA makeup flowrate is not accompanied by a commensurate increase in the $\%CC$ because of the disturbance. Accordingly, this makeup stream is the primary driver of a drastic increase in process economics following the disturbance rejection compared to the initial process cost ($\sim 59{,}000\ \$CAD/yr$ at $t = 0\ h$ to $\sim 1.5M\ \$CAD/yr$ $t \cong 7.5\ h$; Figure 5g and 5b, respectively). That is, despite MEA being seemingly inexpensive per unit volume, the makeup flowrate is drastically elevated as to have a significant negative impact on the economics. The MEA cost as the primary driver of this condition is also confirmed by the similarity of trajectories of process economics and MEA makeup flowrate in Figure 5b and 5i, respectively. For the proposed NMPC structure to reject the large flowrate disturbance, this behaviour is unavoidable as the only way to substantially maintain $\%CC$ on target is through the MEA makeup. These poor steady-state economics last until corrective action is taken by the RTO to find a new suitable set point for the system.

The RTO is executed at $t \cong 8\ h$ to re-optimize the plant economics under the new operating conditions. To achieve the new set points, which in principle represent a more economical operating point, the process must first undergo another dynamic phase while control actions are imposed. These dynamics are observed to be expensive; during this transient, a process cost peak occurs at $t \cong 8.5\ h$, which is caused by a similar peak in the MEA makeup flowrate. The peak occurs as the RTO imposes an increase in $\%CC$ and C_{MEA}^{tank} set points, which are quickly acted upon by an increase in MEA makeup flowrate. This increased cost period is brief, however, and after the dynamics associated with the increase in reboiler duty shown in Figure 5f have elapsed, the MEA makeup decreases back to a near-zero value as the lean loading is decreased through the recycle stream; thus, a large amount of MEA makeup is no longer necessary to maintain the new $\%CC$ set point. These expensive dynamics suggest that the approach presented herein should be applied especially when the system experiences significant and sustained disturbances. The set point increases in $\%CC$ and C_{MEA}^{tank} take advantage of the fact that an increased composition of CO_2 in the flue gas makes it economically advantageous to remove more CO_2 to be sold at the expense of a small increase in reboiler cost, which allows for the reduction of the MEA makeup flowrate as the associated cost. After this initial peak, the controlled variables approach their set point at $t \cong 18\ h$ and the new RTO-defined operating point for the process has a low operating cost of $\sim 48{,}000\ \$CAD/yr$ with respect to the operating cost of pure biomass firing.

The original $\sim 59{,}000\ \$CAD/yr$ (biomass) steady-state cost is broken down into $\sim 86{,}000\ \$CAD/yr$ from reboiler steam, $\sim -32{,}000\ \$CAD/yr$ from CO_2 sales, $\sim 4{,}000\ \$CAD/yr$ from SCC, and $\sim 1{,}000\ \$CAD/yr$ from MEA costs. This is compared to the final $\sim 48{,}000\ \$CAD/yr$ (coal) steady-state cost broken down into $\sim 90{,}000\ \$CAD/yr$ from reboiler steam, $\sim -47{,}000\ \$CAD/yr$ from CO_2 sales, $\sim 5{,}000\ \$CAD/yr$ from SCC, and $\sim 0\ \$CAD/yr$ from MEA costs. This breakdown shows that the RTO increases reboiler duty to achieve more capture (thus sales) despite the increased amount of CO_2 content in the flue gas; this is reflected in an increased reboiler cost and an increased sales profit from the initial to the final steady state. This increased reboiling will typically have implications on the operation of the upstream power plant (e.g. reduction of the power plant's energy output). As a consequence of increased reboiling, the absorber enrichment in the latter (coal-fired) state is primarily achieved through the reboiler rather than the makeup stream, leading to a low MEA makeup cost. The increase in sales profit seen here exemplifies the importance of a carbon economy where CO_2 is treated as a sellable product rather than an unwanted biproduct as noted by [35], thereby encouraging higher capture rates. Moreover, an increase in SCC is observed due to the increased CO_2 content in the flue gas, which leads to more total emissions as reflected in the cost (but less relative emissions considering that more CO_2 is being fed to the absorber). This breakdown reflects the large effect that recoups can have to strengthen the incentive to remove CO_2 as well as make the PCC process more economically feasible. From an energy standpoint, the execution of the RTO increases the reboiler duty from an original $\sim 151{,}800\ W$ to $\sim 157{,}500\ W$. As per equation (21), this increase constitutes approximately a $1315\ \$CAD/h$ decrease in power plant profits, which is entirely justified considering the $\sim 11{,}000 \$CAD/h$ (i.e., $\sim 12\%$ energy penalty) decrease in the optimal steady-state PCC operating cost.

In summary, the net (i.e., including energy penalties) optimal steady state cost for coal is $\sim 19\%$ cheaper than the optimal steady state cost associated with biomass. This occurs as the increased CO_2 content in the flue gas from coal combustion allows for more carbon to be captured and sold at the expense of a minor increase in reboiler duty. Moreover, the evolution of the process economics in this scenario provides new insights with regards to the NMPC and RTO behaviour. The NMPC structure used in this study, while working well to reject disturbances, can lead to drastically increased steady-state operating costs as evidenced in the disturbance rejection phase of the scenario where a significant amount of MEA is required. These high costs, however, are quickly alleviated through the execution of the RTO which lessens the solvent enrichment caused by the MEA makeup and increases the solvent enrichment caused by the reboiler. Moreover, the process dynamics imposed by the NMPC when tracking a new set point can also be expensive because of brief peaks in the MEA makeup; these dynamics are acceptable as they are relatively short-term and are necessary to achieve a more economical operating point. Despite the expensive transients achieved by the proposed scheme, the manipulated variables make a coordinated response as the NMPC is a centralized (multi-variable) control scheme. In contrast, decentralized control strategies would likely lead to even more expensive transient costs as interactions between various control loops would not be accounted for leading to slower control actions; this is a further benefit of the proposed NMPC-based control structure in the case-study. Nevertheless, the losses incurred while operating dynamically to reach a new RTO-defined steady state are justified as they will be recovered in the long term provided that the system is operated at steady state for a sufficiently long period thereafter. For instance, in this case the payback period is $t_{payback} \cong 18\ h$. Moreover, with this control structure, the post-

disturbance steady state costs and dynamic costs are inflated due to the unavailability of reboiler duty as a manipulated variable and the high price of MEA. Lifting this restriction and manipulating the reboiler duty as well as makeup stream would likely shorten the payback period by making the dynamics less expensive; however, this is out of the scope of the present study. Still, the approach proposed in this work was shown effective for the cofiring of fuels, which is an increasingly common operational scheme in fuel-fired power plants, while incurring an acceptable energy penalty.

5.2. Scenario B: diurnal variation of inlet flowrate

It is common for power plants to respond to changing energy demands. Diurnal variation is one case that occurs over the course of the weekday for load-changing power plants, whereby the energy demand of the plant varies cyclically. Peak hours often occur in the late mornings, afternoon, and early night; while low demand occurs the late night, and early mornings. To accommodate cycling energy demands, the quantity of fuel combusted, and thus the quantity of flue gas, both undergo similar diurnal cycles. This scenario has been investigated before [21,29,33,39]. In our previous works [21,29], however, the controller had limited flexibility as it only considered the absorber, thus the solvent could became easily saturated with CO_2, limiting size of disturbances that could be rejected. Through the integration of the control layer in the absorber and buffer tank in this work, larger fluctuations in flue gas flowrate can be rejected as the solvent entering the absorber can be readily concentrated or diluted using the makeup streams.

In this scenario, the cyclic behaviour is modelled as steps around a nominal flue gas flowrate as displayed in Figure 7a; this signal has an amplitude equal to 40% of the nominal flue gas flowrate (i.e., there is a 20% step up and a 20% step down from the nominal flue gas flowrate), which exceeds the amplitude explored in previous studies. Following each disturbance, the controller tracks to its outdated set point. Upon reaching an outdated steady state, the RTO is executed such that an updated operating point is defined. This procedure of disturbance rejection and set point tracking would be repeated daily; for the sake of brevity, only a single cycle is performed in this work.

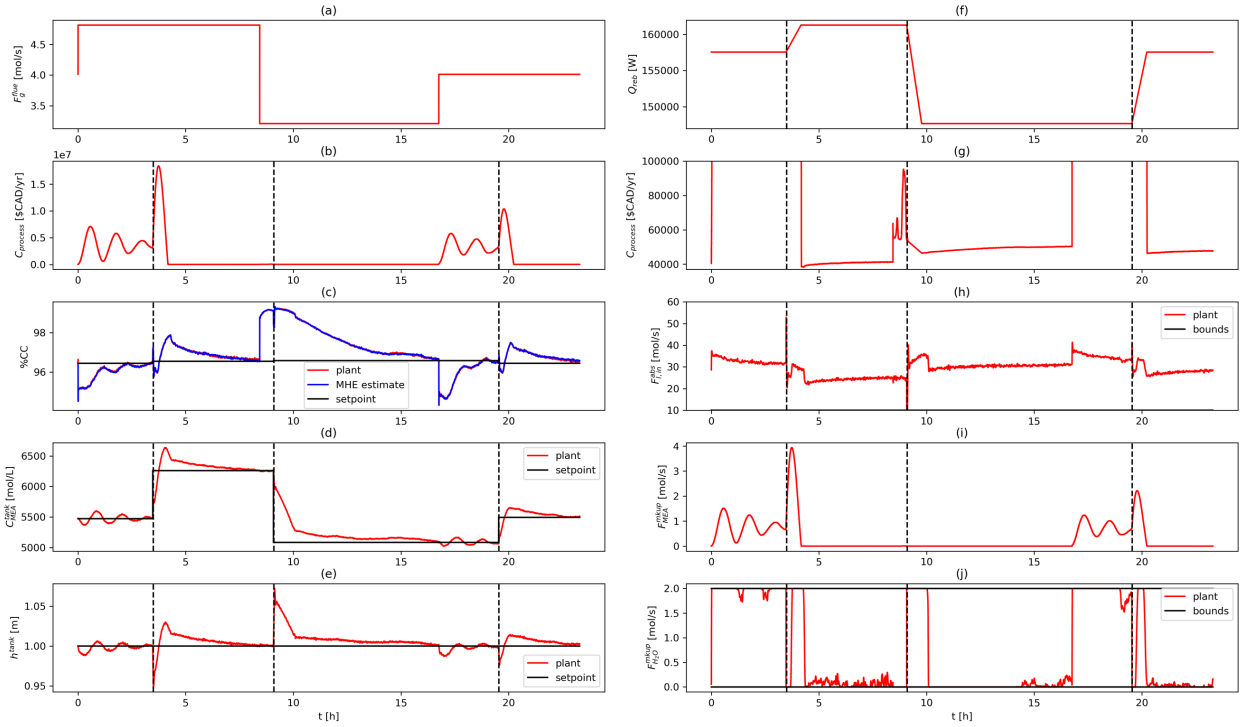

Figure 7: Flue gas flowrate, process cost (b shows full profile, g shows zoomed in profile), controlled variables, and manipulated variables for a diurnal variation scenario. Dashed vertical lines represent times at which the RTO was executed, thus inciting a set point change.

The responses on the buffer tank temperature and cooling duty in this scenario can be found in appendix Figure A4 (Appendix A). For this scenario, the MHE estimates were observed to be in good agreement with the true plant with an $MSE = 7.076 \times 10^{-4}$ and the similar trajectories displayed in Figure 7c. While a 'no-MHE' case was not performed in scenario B as in scenario A for brevity, an MSE on the same order as the scenario A suggests that the MHE performance is similarly good, thus allowing the NMPC to have good performance.

This scenario begins at the economically optimal operating point corresponding to the nominal disturbances outlined in section 3.5. A first disturbance is imposed at $t = 0\ h$ and constitutes a 20% step up in flue gas flowrate, thus beginning the 'peak' hours. Such a disturbance would cause the $\%CC$ to decrease drastically as the amount of solvent being fed into the absorber would no longer be sufficient; however, the disturbance is rejected by the controller through an increase in the MEA makeup flowrate, which enriches the solvent going into the absorber thereby accounting for the excess flue gas. The first disturbance is rejected by $t \cong 4\ h$ with a few brief damped oscillations; however, the resulting process economics are unfavourable because of the new MEA makeup flowrate of $\sim 0.7\ mol/s$ as shown in Figure 7i. This is also reflected in the increase of process cost from $\sim 48{,}000\ \$CAD/yr$ (Figure 7g) pre disturbance rejection to $\sim 3.1M\ \$CAD/yr$ (Figure 7b) post disturbance rejection. At this point ($t \cong 4\ h$), the RTO is executed and leads to a transient lasting until $t \cong 9\ h$, whereby the reboiler duty is increased (Figure 7f) to enrich the recycle stream, thus allowing the system to maintain a high $\%CC$ with a lower makeup flowrate. This quickly reduces the process cost to $\sim 42{,}000\ \$CAD/yr$ (Figure 7g). This new set point is accompanied by an energy penalty to the upstream power plant of $654\ \$CAD/yr$ owed to the increase in reboiler duty; this is acceptable considering the price reduction from

the previous optimal steady state of $\sim 6000\ \$CAD/yr$. Without executing the RTO, the process would have remained at the elevated post-disturbance cost; thus, the cost maintaining the outdated set point (i.e., doing nothing) would be substantial.

At $t \cong 9\ h$, a second 40% step down in flowrate is imposed, thus ending the peak hours. The controller works to reject this disturbance but as shown in Figure 7c, 7d, and 7e, there is a flattening of the controlled variables at $t \cong 10\ h$. At this point, the (40%) step-down disturbance makes the pre-disturbance $\%CC$ set point too low to be reached by the controller as the high reboiler duty elevates the plant $\%CC$. Despite the MEA flowrate being near its lower bound (Figure 7i) and the water flowrate being at its upper bound (Figure 7j), there remains a nearly $2\%CC$ upward offset as the size of the disturbance makes the outdated set point unreachable for the current reboiler duty. In addition to this offset, the system quickly reaches a point where the cost fluctuates noisily as a result of modulation of the MEA makeup near its lower bound (as reflected in Figure 7g at $t \cong 9\ h \rightarrow 10\ h$). This occurs owing to the strong interaction between the MEA makeup and its simultaneous (and conflicting) effect on both the tank level and the $\%CC$. Despite the MEA makeup still varying, it has very little effect on the controlled variables as they are nearly constant by ~10 hours. Moreover, the process cost is still varying at this point with a minimum of $\sim 60{,}000\ \$CAD/yr$. As the controlled variables have flattened by $t \cong 10\ h$, the RTO is executed whereby a new reachable set point is computed and the system undergoes a transient that lasts until $t \cong 17\ h$ hours and reduces the steady-state cost to $\sim 50{,}000\ \$CAD/yr$. The transient associated with this set point change ($t \cong 10\ h \rightarrow 17\ h$) is longer than the previous set point change ($t \cong 4\ h \rightarrow 9\ h$) as the system starts far from its optimal operating point because the previous set point corresponds to a flue gas flowrate that is 40% higher. Despite the new optimal steady state having a cost that is $\sim 8000\ \$CAD/yr$ higher than the previous steady state, the energy penalty incurred to the upstream power plant is $-2385\ \$CAD/yr$ because of the reduction in reboiler duty. In this case, the RTO decision helps the power plant operation as well as the PCC since ~30% of the losses imposed by the new disturbance on the system will be offset by increased power plant profits owing to the reduction of steam being routed to the PCC plant.

At $t \cong 17\ h$, a third 20% step up in flowrate is imposed, thus returning the system to its nominal flue gas flowrate. This disturbance is successfully rejected by $t \cong 20\ h$ but results in another high operating cost of $\sim 2.6M\ \$CAD/yr$ due to the high MEA makeup flowrate of $\sim 0.5\ mol/s$. The RTO is executed again at $t \cong 20\ h$, whereby the process cost is returned to its original $\sim 48{,}000\ \$CAD/yr$ in just under $t \cong 24\ h$, thus completing a cycle. This new set point is accompanied by an energy penalty to the upstream power plant of $1731\ \$CAD/yr$, which is substantial as it negates ~87% of the price reduction from the previous optimal steady-state cost of $\sim 2000\ \$CAD/yr$.

As with the Scenario A, large MEA makeup flowrates following disturbance rejection phases are observed. This re-emphasizes the large economic effects that MEA cost can have despite its relatively low price. In contrast to Scenario A, the disturbances in the present scenario occur relatively frequently, resulting in a plant that is in the disturbance rejection phase more often. This leads to frequent dynamic operation, which was observed to be expensive. Despite this, when the RTO is executed the dynamic process cost (i.e., when a new set point is being tracked) typically decreases drastically following a peak as the NMPC often reduces the MEA makeup quickly.

In the three RTO periods associated with a daylong operation with three disturbances observed in the present scenario, the optimal process cost decreases by $\sim 6000\ \$CAD/yr$, increases by $\sim 8000\ \$CAD/yr$, and decreases by

$\sim 2000\ \$CAD/yr$ for each RTO period, respectively. The first cost decrease is enabled by the increase in flue gas flowrate, which allows for substantially more carbon to be captured and sold per unit time with only a slight increase in reboiler duty. It is associated with a sizable net (considering energy penalty) cost improvement of $\sim 12\%$ with respect to the pre-disturbance process cost. The second RTO period and its associated increase in cost occurs because of the significant decrease in flue gas flowrate, which allows for less sales recoups. Despite this, the RTO still enables the reduction of steady state cost from the post-disturbance steady state by $\sim 17\%$; that is, while there is an increase of steady state cost with respect to the previous disturbance in this case, the RTO still results in significant loss abatement from the second disturbance-rejection phase. Furthermore, the third RTO period observed a more modest $\sim 0.6\%$ of net cost improvement over the previous RTO period because of a large energy penalty as noted above. Dynamically, for the three RTO periods observed in this scenario, the payback periods were calculated to be $t_{payback} \cong 8\ h$, $t_{payback} \cong 12\ h$, and $t_{payback} \cong 7\ h$ in chronological order. Thus, none of the RTO periods are operated at steady state for a sufficiently long time to justify the expensive dynamics as the payback period is not completed before a new disturbance is imposed. For a scenario such as this where the system has little time to settle before more disturbances are imposed, an EMPC structure may be more well-suited for the dynamic costs to be considered; however, EMPC also has disadvantages as stated in the introduction. Nevertheless, this scenario showed that the execution of the RTO decreased the steady-state costs from the disturbance-rejection phase cost in all three RTO periods observed herein, and that the scheme can handle very large disturbances in flue gas flowrate (with the caveat of expensive dynamics). For slower power plants that do not impose such large load changes on the PCC process, this approach would be more suitable. Moreover, the energy penalty of the power plant was relatively small or negative for two of the RTO periods; even when the penalty was large, it did not exceed the savings incurred by the RTO.

5.3. Scenario C: variation in prices

To assess the effect of the pricing of RTO economic cost terms on the system's operation, disturbances were imposed on the prices associated with the two primary cost terms (i.e., those that incur the biggest profit or loss during nominal operation as established in the cost breakdown in scenario A). Accordingly, the largest contributors to the overall cost were found to be the reboiler steam cost and CO_2 sales profit. These prices were varied within ±10% of their nominal value in a series of steps over five RTO periods as depicted in Figure 8a.

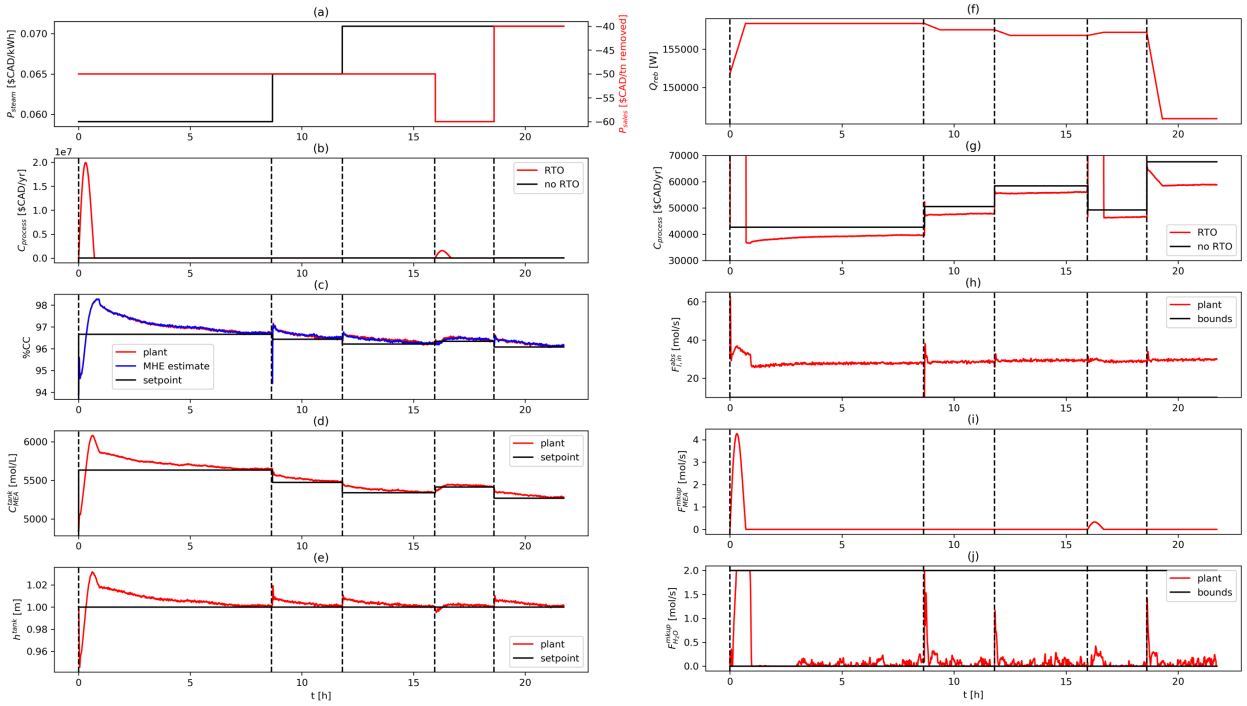

Figure 8: Price profiles, process cost, controlled variables (b shows full profile, g shows zoomed in profile), and manipulated variables for price variation scenario. Dashed vertical lines represent times at which the RTO was executed, thus inciting a set point change.

The responses on the buffer tank temperature and cooling duty in this scenario can be found in appendix Figure A5 (Appendix A). As with the previous scenarios, the MHE estimates were observed to be in good agreement with the true plant with an $MSE = 1.075 \times 10^{-3}$. Moreover, a 'no-MHE' case was performed for this scenario as summarized in Appendix A (Figure A6) and Appendix B (Table B3). The control and economic performance loss in this scenario were found to be similarly small to that observed in Scenario A; hence, it is deemed acceptable under the assumptions considered for the present MHE scheme.

The starting point for this scenario corresponds to the nominal conditions outlined in section 3.5 and Table B1 (Appendix B), in which the system starts far from its economically optimal steady state as reflected in the long initial transient (~8.5 hours) in $\%CC$, C_{MEA}^{tank}, and h^{tank} (Figure 8c, 8d, and 8e, respectively). Once the system reaches its new operating condition at the end of this transient, the subsequent dynamics related to price changes are comparatively short as they represent adjustments near the optimum rather than a move into a radically different operating point. This is reflected in the small magnitude of the adjustments and brief dynamics made on the $\%CC$ and h^{tank} in RTO periods 2–5.

Figure 8b and g show the process cost after execution of the RTO with updated pricing and the subsequent tracking to the newly defined set points that were observed. This profile is compared to the process cost profile of a 'no RTO' case (also shown in Figure 8b and 8g) where the controlled and manipulated variables are maintained at their nominal values (i.e., $\boldsymbol{Y_{nom}}$ and $\boldsymbol{u_{nom}}$, respectively). This way, the economic benefit of executing the RTO over remaining at the nominal operating conditions suggested in the literature [38] can be assessed. The RTO always supplies economically advantageous operating points; however, the amount of improvement over the nominal scenario depends

on the specific pricing as summarized in Table 10. These improvements range from modest (RTO period 3, nominal sales prices and high reboiler price) to substantial (RTO period 5, low sales price and high reboiler price).

Table 10: PCC savings, energy penalty, and net savings for different RTO periods (price combinations) with respect to the 'no RTO' case

RTO period	**PCC savings** ($\$CAD/yr$)	**Energy penalty** ($\$CAD/yr$)	**Net savings (%)**
1	3047	1149	4.45
2	2776	1005	3.50
3	2417	876	2.64
4	2608	946	3.38
5	8742	−1032	14.47

The second and third RTO periods, after the system reaches its first economic optimum and only reboiler prices are disturbed, provide modest economic advantages over the 'no RTO' operation. This suggests the economic optimum is only mildly dependent on the price of steam although steam comprises a large part of the total cost. The importance of steam price is corroborated by the increase in cost from $\sim 39{,}000\ \$CAD/y$ to $\sim 56{,}000\ \$CAD/y$ upon the two steam price increases, which represents a significant economic penalty. In other words, the reboiler cost makes up a large part of the process economics, but the RTO can only provide modest improvements to offset changes in this price if the system begins at an optimum. Nevertheless, these improvements are worthwhile if the price holds for a long time thereafter. These increases in reboiler cost also cause the RTO to generate lower $\%CC$ set points as the removal of $\%CC$ is disincentivized since it becomes more expensive for the reboiler to provide a MEA-rich recycle stream. Moreover, with the reboiler prices increasing during the second and third RTO periods, the system experience successive decreases in savings and energy penalty. The energy penalty to the power plant is decreased as the RTO dictates that less duty is required as the steam price becomes more expensive while the PCC savings also decrease as less carbon is captured as a result. In both periods, the decreases in PCC savings outpaces the decreases in energy penalty, resulting in lower net savings.

During the fourth RTO period in which the sales price is increased, an increasing incentive to remove CO_2 is observed through a slight increase in $\%CC$ set point. This occurs along with a significant drop in process cost to $\sim 46{,}000\ \$CAD/y$ as more economic benefits can be recouped through CO_2 sales. This period also represents an increase in the improvement over the no RTO case from the previous period as displayed in Table 10, which suggests that there is a larger economic benefit to be gained by executing the RTO upon sales prices changes. In this fourth period, the energy penalty increases owing to the increased recoup price, which incentivizes removal and higher reboiler duty. In contrast to the previous two periods, the increase in PCC savings is greater than the increase in energy penalty, hence an increase in net savings is observed.

The notion of potentially large savings to be made upon changes in sales price is further reinforced in the fifth RTO period, which represents the most substantial cost improvement over the 'no RTO' case. This occurs with a low sales price, which decreases the $\%CC$ set point by drastically decreasing the reboiler duty leading to a large price increase. In this period, the RTO allows less CO_2 to be removed since the economic incentive of selling the capture material is

significantly reduced. This is reflected in the process economics as there is a decrease in the money recouped through sales, causing the process cost to increase to a high of $\sim 65{,}000\ \$CAD/y$. A substantial decrease in reboiler duty such that it goes below the reboiler duty in the 'no RTO' case is dictated by the RTO in this period; hence the negative energy penalty as shown in Table 10. In this case, the savings are substantial as they are made with respect to both the PCC and the power plant, hence the large net savings.

As observed in this scenario, there can be a significant dependence of optimal process cost on the material and energy prices as shown in Figure 8g ranging from $\sim 39{,}000\ \$CAD/y$ to $\sim 56{,}000\ \$CAD/y$. However, these all represented improvements with respect to the nominal operating point reported by Nittaya [38] with net savings ranging from $\sim 3 - 14\%$ as summarized in Table 10 (i.e., net because the associated energy penalties are accounted for). As in previous scenarios, the dynamics associated with some set point changes were observed to be costly during some periods of time. This was observed at the beginning of RTO periods 1 and 4 where there are short (~ 40 minute) spikes in MEA makeup. Accordingly, the RTO should be primarily executed if the prices are expected to hold thereafter such that the detriment from the spikes can be made up for by the improved steady-state economics. As in the previous scenarios, the energy penalty to the power plant never exceeded the RTO savings, thus justifying the use of an RTO framework. Day-to-day variations in typical commodity/energy prices are often noisy and small, thus they would not warrant set point changes. In contrast, price variation on the order observed in this scenario (i.e., $\pm 10\%$) would occur less regularly; these would warrant the execution of the RTO as doing nothing would represent significant additional costs as shown by the comparison to the no RTO case in Table 10. That is, large price changes as observed in this scenario are outside the tolerance of noise and occur when there is a market change; these price changes would justify the use of RTO such that the payback period is short given the expensive dynamics observed.

The averaged computational times for the RTO, NMPC, and MHE in the proposed scheme for this scenario are $4.33\ s$, $55.43\ s$, and $64.65\ s$, respectively. The CPU times do not change significantly across test scenarios as the optimization problems are of the same size and were carried out using the same hardware; thus, these times are representative for all scenarios. As can be observed in the CPU times for the dynamic optimization problems, the implementation of a large model as in the present study requires significant computational effort; this is one of the drawbacks of using a mechanistic model. Despite having the same number of equations, the MHE problem requires more CPU time than the NMPC problem, owing to an increased number of decision variables (i.e., manipulated variables trajectories in NMPC vs. state trajectories in MHE). The long computational times of the dynamic optimization problems used herein warrant adjustments in the solution strategy for the scheme to be used in a real plant. One option is to accept the computational delay caused by these long CPU times and asses its effect on the control and estimation layers; however, this can have detrimental effects on performance. Previous studies have proposed the use of terminal conditions to mitigate this issue [54], but this increases the implementational complexity of the control scheme. More attractively, a reduction in this computational effort can be achieved through efficient reformulations such as the advanced-step NMPC presented by [55].

5.4. Remarks

The scheme was implemented on an MEA-solvent pilot-scale PCC absorber section and a mechanistic process model was used for the layers comprised in the proposed scheme. The absorber section and proposed scheme were subjected

to test scenarios including cofiring, diurnal variations, and price variations to assess performance. A ~19% improvement in process cost was observed in the cofiring scenario (A) with only a small (~0.5%) of economic performance deterioration caused by the MHE. The diurnal variation scenario (B) revealed improvement in steady-state economics upon the introduction of each new disturbance from ~12% cost improvements (in the cases where disturbances caused the cost to improve) to ~17% loss abatement (in the cases where the disturbances caused the cost to increase). Furthermore, a ~3% to ~14% cost improvement with respect to maintaining a constant set point was observed for different economic incentives (through price variations) in the scenario C.

Dynamically, the NMPC layer was shown to track the RTO-supplied economically optimal set points quickly in all scenarios while maintaining non-economic variables, such as temperature and level, steady. Occasionally, the control actions in the NMPC were observed to be expensive because of the use of MEA makeup as a manipulated variable; this would make the proposed scheme expensive to execute for plants subject to continuous disturbances where steady-state operation is not sustained for long periods. This finding is consistent with the fact that RTO is a steady-state optimization method, which does not consider dynamics when determining set points. Nevertheless, the payback periods for the scenarios observed in this work were found to be reasonable with respect to the RTO period lengths (i.e., the payback period were of similar lengths to the RTO periods). Moreover, the MHE was observed to provide consistently acceptable estimates of the absorber as observed through the NMPC performance, which showed little deterioration compared to when full state access was assumed. The fidelity of the estimates was also evidenced by the low error in the MHE-estimated $\%CC$ with respect to the true $\%CC$.

From a process economics perspective, it was found through the test scenarios that there is a substantial potential to recoup costs through CO_2 sales; this was most salient at high inlet CO_2 concentrations (i.e., with very emissive fuels) and high flue gas throughputs, whereby the PCC plant was operated at a high $\%CC$. Furthermore, the energy penalty to the upstream power plant was always lower than the economic benefit incurred by the RTO; thus, justifying the execution of the RTO even if the energy consumption led to some reduction of its potential cost improvements. It is thus evident that the RTO, while not having a model of the power plant, is able to make sensible decisions regarding the energy use of the PCC plant such that the power plant does not experience an undue energy burden because of carbon capture.

6. Conclusions and future work

A novel operational scheme was proposed and implemented for PCC plants. This includes RTO, NMPC, and MHE layers. The RTO layer introduces a novel economic function, which provides a comprehensive consideration of process economics through its inclusion of SCC, CO_2 sales profit, chemical cost, and energy cost; this provides realistic and economical set points to the control layer through its use of the proposed economic function. The NMPC layer enables the centralized control of the absorber and buffer tank while keeping the system inside its physical and safety constraints. Moreover, the control structure in the case study provides adequate control flexibility because of its ability to concentrate and dilute the absorber feed using the buffer tank makeup streams. The MHE layer provides accurate estimates of the states required to execute the previous two layers while only requiring a realistic number of measurements and ensuring that the estimates adhere to constraints. The case study results demonstrate that the operational approach presented herein do, in fact, provide an economically optimal operating approach for PCC

operating downstream from fuel-fired power plants. Approaches such as this will be paramount in achieving economic viability in PCC such that fuel-firing can become environmentally viable.

The following insights were obtained from this study:

- The RTO was found to provide consistent steady-state cost improvements across all scenarios tested.
- The cost improvements always exceeded the energy penalty imposed on the upstream power plant by the PCC plant; resulting in net gains despite any additional energy expended.
- The MEA cost was found to be large following disturbance rejection and when operating dynamically. Conversely, the MEA cost was found to be low when operating at the RTO-defined set points while allowing for low reboiler duty to be necessary. CO_2 sales were found to significantly lessen the process cost in all scenarios.
- The MHE was found to provide acceptable estimates to the NMPC, leading to good control performance that resulted in economically attractive operating points.
- The NMPC was observed to perform well under an array of large disturbances through its use of the makeup streams and its coordination of control objectives.

Despite the evident advantages of this operational approach, there remain assumptions and limitations that must be addressed for this operational scheme to be implementable. Namely, the significant effect of the stripper reboiler in terms of cost was observed in this study through a simplified model. This finding warrants further investigation as to how the explicit inclusion of the reboiler could aid the control layer in conjunction with MEA makeup manipulation as proposed herein. Additionally, the loss of power plant efficiency resulting from steam used in reboiler heating also needs to be studied.

As further evidenced in the results, there exists a trade-off between changing the set point and the dynamics that ensue as a result, which are often expensive. These economic trade-offs and the computational effort involved should be compared to those frameworks that consider the process economics in the transient domain, i.e., EMPC. By adapting the novel economic function proposed herein to a dynamic optimization problem that considers transient costs in an approach like EMPC, a more comprehensive understanding of the connection between dynamics and process cost could be established. Moreover, steady state and dynamical operational approaches can then be compared such that the best PCC operational schedules and schemes can be determined for different power plant operational scenarios.

Plant-model uncertainty is assumed to be negligible in this study and this assumption should be relaxed in future works. [21] showed the applicability of a robust multi-scenario controller for the absorber, which could be extended to include the buffer tank model. A similar multi-scenario approach to that used in [21] could also be used in the MHE, NMPC, and RTO. Alternatively, a parameter estimation problem for the system could be solved; thus, providing updated parameter estimates for the model layers. Corrosion is also assumed to be negligible in the present study but is an important factor preventing the uptake of PCC. A suitable control approach that explicitly models corrosion as noted in [56], could potentially mitigate these effects by considering corrosion minimization as an additional operational incentive; this will be a topic of future work.

Lastly, as the mechanistic model used in this work was developed using data from a pilot plant and, accordingly, the operating conditions, dynamics, and cost reflect this scale. In the future, a scale-up of this model must be performed

to assess the operational advantages of the scheme in an industrial system. The results obtained from this work also reflect the current economic incentives as manifested in the prices used. With scaled-up conditions as well as future process developments that change the economic incentives (e.g., energy-efficient solvents, increased carbon prices, decreased energy prices), the process can be re-optimized and reassessed through the economic framework developed in this work, thus resulting in an optimal operation that can simultaneously capture CO_2 at low operational costs.

Acknowledgements

The authors would like to acknowledge the Natural Sciences and Engineering Research Council of Canada (NSERC) for their financial support.

Nomenclature

Operational scheme		**PCC process**	
Symbols			
Control horizon	C	Wetted area of absorber (m^2/m^3)	a_w
Disturbance variables	$\boldsymbol{d}$	Unit cross-sectional area (m^2)	A
Mechanistic model	$\boldsymbol{f}$	Molar specific heat capacity	c_p
Inequality constraints	$\boldsymbol{g}$	Concentration (mol/L)	C
Observation model	$\boldsymbol{h}$	Unit diameter (m)	D
Estimation window	N	Molar flowrate (mol/s)	F
Prediction horizon	P	Unit height (m)	h
Weighting matrix	$\boldsymbol{Q}$	Heat loss coefficient	h_{loss}
Weighting matrix	$\boldsymbol{R}$	Lean loading (mol/mol)	LL
Time	t	Mass flowrate (tn/s)	$\dot{m}$
Manipulated variables	$\boldsymbol{u}$	Molar holdup (mol)	n
States	$\boldsymbol{x}$	Molar flux ($mol/m^2/s$)	N
State estimates/predictions	$\widehat{\boldsymbol{x}}$	Column pressure (kPa)	p
Algebraic variables	$\boldsymbol{y}$	Price ($\$CAD/unit$)	P
Algebraic variable predictions	$\widehat{\boldsymbol{y}}$	Duty (W)	Q
Controlled variables	$\boldsymbol{Y}$	Fluid temperatures (K)	T
Controlled variable predictions	$\widehat{\boldsymbol{Y}}$	Fluid velocity (m/s)	u
Measurements	$\boldsymbol{z}$	Gas molar fraction	y
Measurement noise	$\boldsymbol{v}$	Column height (m)	z
Arrival cost	$\boldsymbol{\varphi}$	Enthalpy (J/mol)	ΔH
Process noise	$\boldsymbol{w}$	Density (mol/L)	ρ
		Percent carbon capture	$\%CC$
Subscripts and superscripts			
Annum/year	$annum$	Absorber	abs
Controller	c	Ambient	amb
Dynamic	d	Captured by absorber	cap
Estimated quantity/estimation	e	Chemical feeds	$chem$
Final time	f	Buffer tank cooling	$cool$
Filtered quantity	F	Chemical components/species	$comp$
Finite elements in column height domain	fez	Carbon dioxide	CO_2
Upper bound	h	Electricity sold to consumers	$elec$
Lower bound	l	Energy consumption	$energy$
Measured quantity	m	Flue gas stream	$flue$
Moving horizon estimation	MHE	Gas	g
Mean squared error	MSE	Top of absorber column	H
Nonlinear model predictive control	$NMPC$	Water	H_2O
Payback (period)	$payback$	Into unit	in
PCC process case study	$process$	Liquid	l
Post-combustion capture	PCC	Makeup stream	$mkup$
Real-time optimization	RTO	Monoethanolamine	MEA
Steady-state	s	Nominal	nom
Set point	sp	Nitrogen gas	N_2
Sum of squared errors	$\boldsymbol{SSE}$	Out of unit	out
Current time period	t	Reboiler heating	reb
True (i.e., not estimated) quantity	T	Recycle stream	rec
Initial condition/time	0	Reaction	rxn
		Captured carbon sales	$sales$
		Steam generated by power generation	$steam$

		Buffer tank	$tank$
		Vaporization of water	vap
		Emitted from absorber in vent gas	$vent$
		Bottom of absorber column	0

Appendix A

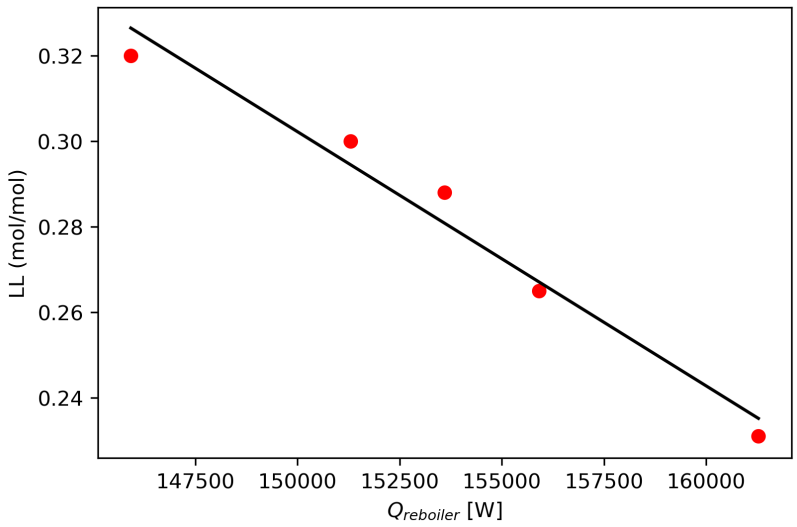

Figure A1: Data and linear regression fit for recycle lean loading duty correlation.

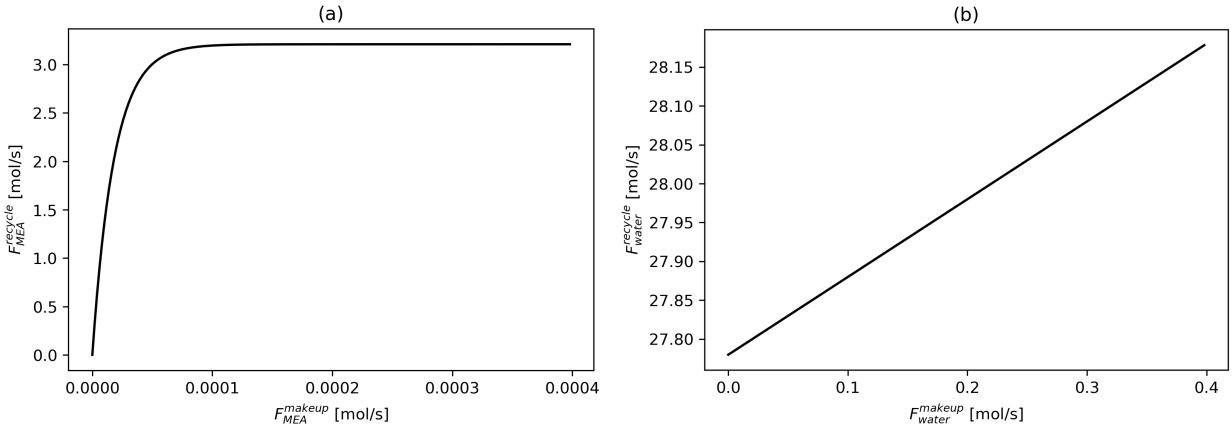

Figure A2: Recycle stream correlations for a) MEA b) water, assuming nominal water content in the flue gas

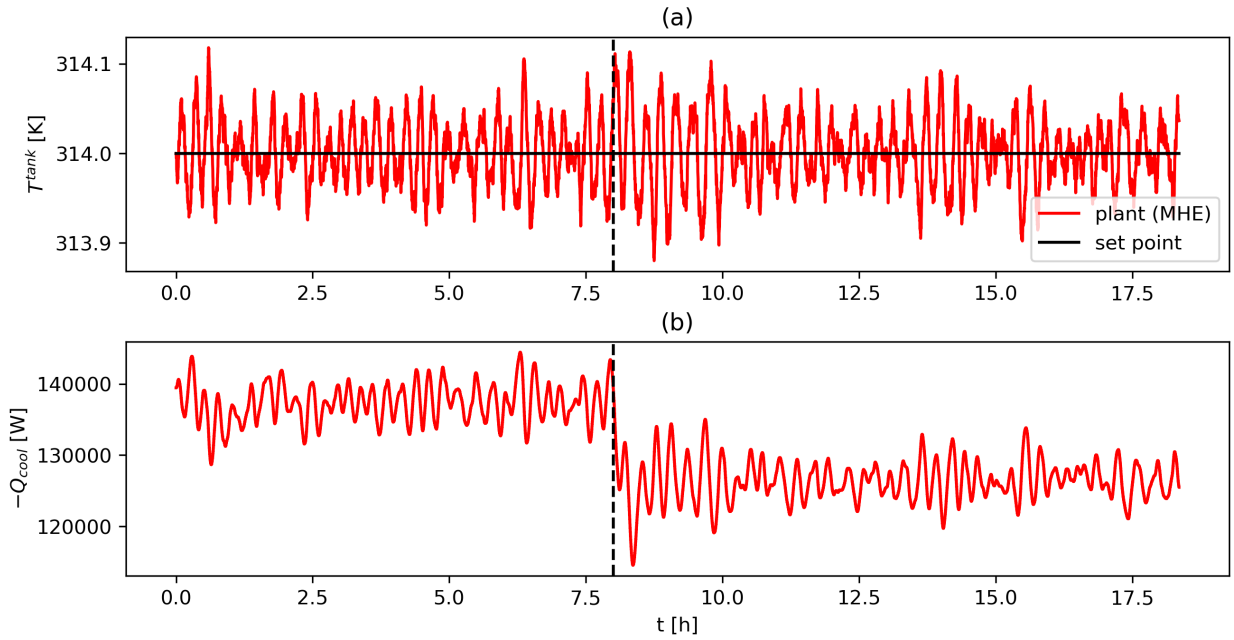

Figure A3: Scenario A plots of a) tank temperature and b) cooling duty. Dashed lines denote RTO executions.

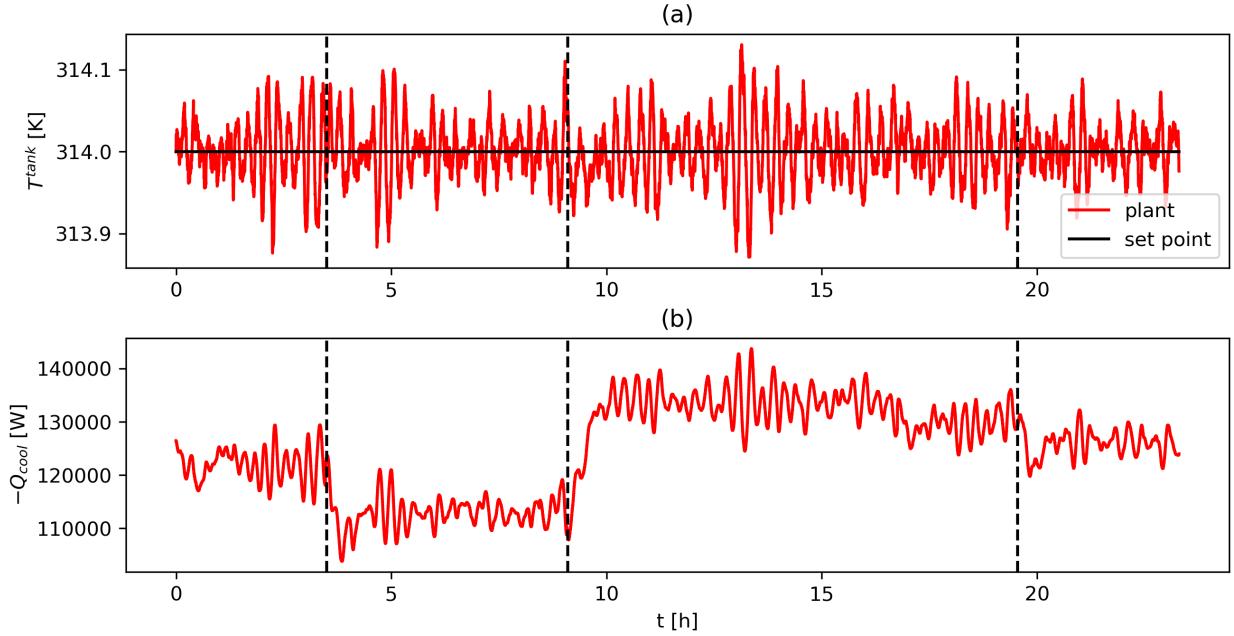

Figure A4: Scenario B plots of a) tank temperature and b) cooling duty. Dashed lines denote RTO executions.

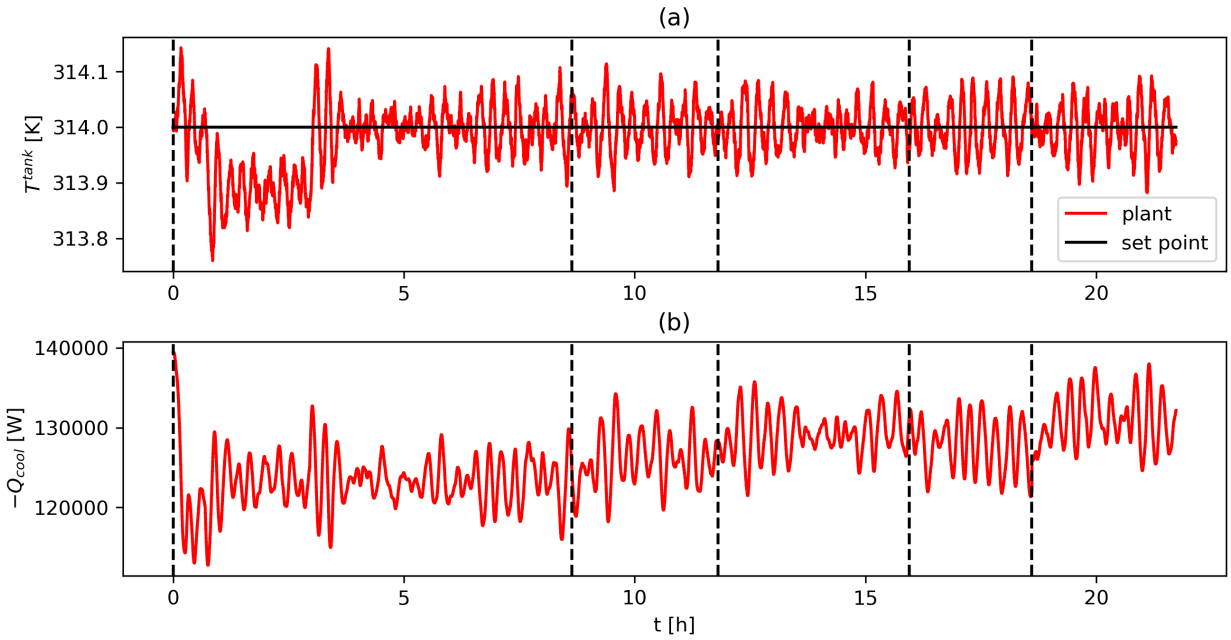

Figure A5: Scenario C plots of a) tank temperature and b) cooling duty. Dashed lines denote RTO executions.

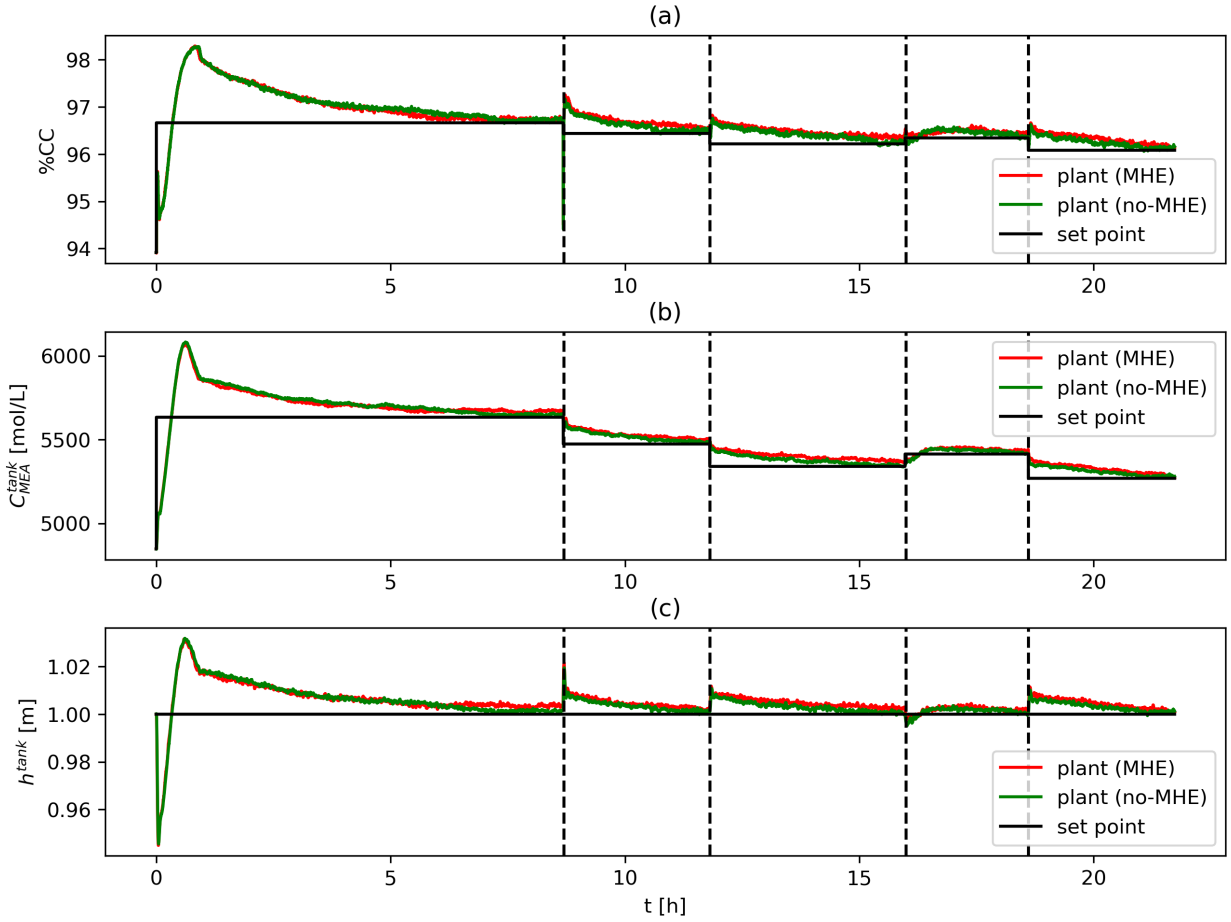

Figure A6: Controlled variables in MHE and no-MHE cases for Scenario C. Dashed lines denote RTO executions.

Appendix B

Table B1: Nominal stream conditions for the present model.

	Recycle stream	**Fresh MEA**	**Fresh water**	**Tank outlet (lean solvent)**	**Flue gas**	**Vent gas**	**Rich solvent**
Temperature (K)	366.50	298.00	298.00	314.00	319.71	314.06	318.43
Flowrate (mol/s)							
MEA	3.2098	0.0002	0.0000	3.2100	0.0000	0.0000	3.2098
CO_2	0.9800	0.0000	0.0000	0.9800	0.7020	0.0427	1.6393
Water	27.780	0.0000	0.2000	27.980	0.1000	0.2340	27.846
N_2	0.0000	0.0000	0.0000	0.0000	3.2100	3.2100	0.0000
Total	31.9698	0.0002	0.2000	32.170	4.0120	3.4869	32.6951

Table B2: Validation cases and conditions for the present model against data from [42].

						Composition (mol/mol)			
Case #		**Temperature (K)**		**Flowrate (mol/s)**		**Lean solvent**	**Flue gas**		
Current study	[42]	Lean solvent	Flue gas	Lean solvent	Flue gas	LL	Water	CO_2	Packing height (m)
1	32	314	320	29.0	3.52	0.279	0.013	0.177	5.00
2	43	313	327	29.3	5.28	0.231	0.022	0.170	7.80
3	28	313	321	58.2	7.07	0.287	0.016	0.165	5.85
4	39	313	328	60.0	7.02	0.228	0.016	0.169	6.10

Table B3: Effect of MHE on control and economic performance for scenario C.

Controlled variable	***SSE*** **(MHE)**	***SSE*** **(no-MHE)**	**Performance loss** (%)
$\%CC$ (%)	5240	4975	5.327
C_{MEA}^{tank} (mol/L)	2.747×10^8	2.732×10^8	0.549
$h^{tank}(m)$	1.704	1.628	4.668
Economics	**Cost (MHE)**	**Cost (no-MHE)**	
$\int_0^{18h} C_{process} dt$ $(\$CAD)$	4790	4636	3.322

References

[1] IEA. Key World Energy Statistics 2020. IEA 2020. [Online] https://www.iea.org/reports/key-world-energy-statistics-2020.

[2] Theo WL, Lim JS, Hashim H, Mustaffa AA, Ho, WS. Review of pre-combustion capture and ionic liquid in carbon capture and storage. Appl. Energy. 2016;183:1633–1663. https://doi.org/10.1016/j.apenergy.2016.09.103.

[3] Wang Y, Zhao L, Otto A, Robinius M, Stolten D. A Review of Post-combustion CO2 Capture Technologies from Coal-fired Power Plants. Energy Procedia. 2017;114:650–665. https://doi.org/10.1016/j.egypro.2017.03.1209.

[4] Lucio M, Ricardez-Sandoval L. Dynamic modelling and optimal control strategies for chemical-looping combustion in an industrial-scale packed bed reactor. Fuel. 2019;262:116544. https://doi.org/10.1016/j.fuel.2019.116544.

[5] You H, Yuan Y, Li J, Sandoval L. A multi-scale model for CO2 capture: A nickel-based oxygen carrier in chemical-looping combustion. IFAC-PapersOnLine. 2018;51(18):97–102. https://doi.org/10.1016/j.ifacol.2018.09.264.

[6] Chansomwong A, et al. Dynamic modelling of a CO2 capture and purification unit for an oxy-coal-fired power plant. Int. J. Greenh. Gas Control. 2014;22:111–122. https://doi.org/10.1016/j.ijggc.2013.12.025.

[7] Dugas E. Pilot plant study of carbon dioxide capture by aqueous monoethanolamine. Masters thesis. University of Texas at Austin; 2006.

[8] Idem R, et al. Pilot plant studies of the CO2 capture performance of aqueous MEA and mixed MEA/MDEA Solvents at the University of Regina CO2 capture technology development plant and the boundary dam CO2 capture demonstration plant. Ind. Eng. Chem. Res. 2006;45(8):2414–2420. https://doi.org/10.1021/ie050569e.

[9] Huang B, et al. Industrial test and techno-economic analysis of CO2 capture in Huaneng Beijing coal-fired power station. Appl. Energy. 2010;87(11):3347–3354. https://doi.org/10.1016/j.apenergy.2010.03.007.

[10] Monañes RM, Flø NE, Nord LO. Experimental results of transient testing at the amine plant at Technology Centre Mongstad: Open-loop responses and performance of decentralized control structures for load changes. Int. J. Greenh. Gas Control. 2018;73:42–59. https://doi.org/10.1016/j.ijggc.2018.04.001.

[11] Danaci D, Bui M, Petit C, Mac Dowell N. En Route to Zero Emissions for Power and Industry with Amine-Based Post-combustion Capture. Environ. Sci. Technol. 2021. https://doi.org/10.1021/acs.est.0c07261.

[12] Li K, Leigh W, Feron P, Yu H, Tade M. Systematic study of aqueous monoethanolamine (MEA)-based CO2 capture process: Techno-economic assessment of the MEA process and its improvements. Appl. Energy. 2016;165:648–659. https://doi.org/10.1016/j.apenergy.2015.12.109.

[13] Luu MT, Abdul Manaf N, Abbas A. Dynamic modelling and control strategies for flexible operation of amine-based post-combustion CO 2 capture systems. Int. J. Greenh. Gas Control. 2015;39:377–389. https://doi.org/10.1016/j.ijggc.2015.05.007.

[14] Mechleri E, Lawal A, Ramos A, Davison J, MacDowell N. Process control strategies for flexible operation of post-combustion CO2 capture plants. Int. J. Greenh. Gas Control. 2017;57:14–25. https://doi.org/10.1016/j.ijggc.2016.12.017.

[15] Panahi S, Skogestad S. Economically efficient operation of CO2 capturing process. Part II. Design of control layer. Chem. Eng. Process. 2012;52:112–124. https://doi.org/10.1016/j.cep.2011.11.004.

[16] Jung H, Heo S, Lee JH. Model predictive control for amine-based CO_2 capture process with advanced flash stripper. Control Eng. Pract. 2021;114:104885. https://doi.org/10.1016/j.conengprac.2021.104885.
[17] He Z, Hossein Sahraei M, Ricardez-Sandoval LA. Flexible operation and simultaneous scheduling and control of a CO_2 capture plant using model predictive control. Int. J. Greenh. Gas Control. 2016;48:300–311. https://doi.org/10.1016/j.ijggc.2015.10.025.
[18] Jung H, Im D, Heo S, Kim B, Lee JH. Dynamic analysis and linear model predictive control for operational flexibility of post-combustion CO2 capture processes. Comput. Chem. Eng. 2020;140:106968. https://doi.org/10.1016/j.compchemeng.2020.106968.
[19] Åkesson J, et al. Nonlinear model predictive control of a CO2 post-combustion absorption unit. Chem. Eng. Technol. 2012;35(3):445–454. https://doi.org/10.1002/ceat.201100480.
[20] Akinola O, Oko E, Wu X, Ma K, Wang M. Nonlinear model predictive control (NMPC) of the solvent-based post-combustion CO2 capture process. Energy. 2020:213;118840. https://doi.org/10.1016/j.energy.2020.118840.
[21] Patrón GD, Ricardez-Sandoval LA. A robust nonlinear model predictive controller for a post-combustion CO_2 capture absorber unit. Fuel. 2020;265:116932. https://doi.org/10.1016/j.fuel.2019.116932.
[22] Altan A, Karasu S, Zio E. A new hybrid model for wind speed forecasting combining long short-term memory neural network, decomposition methods and grey wolf optimizer. Appl. Soft Comp. 2021;100:106996. https://doi.org/10.1016/j.asoc.2020.106996.
[23] Karasu S, Altan A, Bekiros S, Ahmad W. A new forecasting model with wrapper-based feature selection approach using multi-objective optimization technique for chaotic crude oil time series. Energy. 2020;212:118750. https://doi.org/10.1016/j.energy.2020.118750.
[24] Rangel-Martinez D, Nigam KDP, Ricardez-Sandoval L. Machine learning on sustainable energy: A review and outlook on renewable energy systems, catalysis, smart grid and energy storage. Chem. Eng. Res. Des. 2021;174:414–441. https://doi.org/10.1016/j.cherd.2021.08.013.
[25] Wang H, Ricardez-Sandoval LA. Dynamic optimization of a pilot-scale entrained-flow gasifier using artificial recurrent neural networks. Fuel. 2020;272:117731. https://doi.org/10.1016/j.fuel.2020.117731.
[26] Helei L, Tantikhajorngosol P, Chan C, Tontiwachwuthikul P. Technology development and applications of artificial intelligence for post-combustion carbon dioxide capture: Critical literature review and perspectives. Int. J. Greenh. Gas Control. 2021;108:103307. https://doi.org/10.1016/j.ijggc.2021.103307.
[27] Rahimi M, Moosavi SM, Smit B, Hatton TA. Toward smart carbon capture with machine learning. Cell Rep. Phys. Sci. 2021;2(4):100396. https://doi.org/10.1016/j.xcrp.2021.100396.
[28] Salvinder K, et al. An overview on control strategies for CO2 capture using absorption/stripping system. Chem. Eng. Res. Des. 2019;147:319–337. https://doi.org/10.1016/j.cherd.2019.04.034.

[29] Patrón GD, Ricardez-Sandoval L. Real-Time Optimization and Nonlinear Model Predictive Control for a Post-Combustion Carbon Capture Absorber. IFAC-PapersOnLine. 2020;53(2):11595–11600. https://doi.org/10.1016/j.ifacol.2020.12.639.

[30] Yin X, Decardi-Nelson B, Liu J. Distributed monitoring for the absorbtion column of a post-combustion CO_2 capture plant. Int. J. Adapt. Control Signal Process. 2019;34(6):757-776. https://doi.org/10.1002/acs.3074.

[31] Chan LLT, Chen J. Economic model predictive control of an absorber-stripper CO2 capture process for improving energy cost. IFAC-PapersOnLine. 2018;51(18):109–114. https://doi.org/10.1016/j.ifacol.2018.09.284.

[32] Decardi-Nelson B, Liu S, Liu J. Improving flexibility and energy efficiency of post-combustion CO2 capture plants using economic model predictive control. Processes. 2018;6(9):135. https://doi.org/10.3390/pr6090135.

[33] Akula P, Eslick J, Bhattacharyya D, Miller DC. Model Development, Validation, and Optimization of an MEA-Based Post-Combustion CO_2 Capture Process Under Part-Load and Variable Capture Operations. Ind. Eng. Chem. Res. 2021;60(14):5176–5193. https://doi.org/10.1021/acs.iecr.0c05035.

[34] Ellis M, Durand H, Christofides PD. A tutorial review of economic model predictive control methods. J. Process Control. 2014;24(8):1156–1178. https://doi.org/10.1016/j.jprocont.2014.03.010.

[35] Nwaoha C, Tontiwachwuthikul P. Carbon dioxide capture from pulp mill using 2-amino-2-methyl-1-propanol and monoethanolamine blend: Techno-economic assessment of advanced process configuration. Appl. Energy. 2019; 250:1202–1216. https://doi.org/10.1016/j.apenergy.2019.05.097.

[36] Rhinehart R. Automated steady state and transient state identification in noisy processes. American control conference. 2013. 10.1109/ACC.2013.6580530.

[37] Valipour M, Ricardez-Sandoval LA. Assessing the Impact of EKF as the Arrival Cost in the Moving Horizon Estimation under Nonlinear Model Predictive Control. Ind. Eng. Chem. Res. 2021;60(7):2994–3012. https://doi.org/10.1021/acs.iecr.0c06095.

[38] Nittaya T. Dynamic Modelling and Control of MEA. Masters thesis. University of Waterloo; 2014. http://hdl.handle.net.proxy.lib.uwaterloo.ca/10012/8128.

[39] Harun N, Nittaya T, Douglas P, Croiset E, Ricardez-Sandoval L. Dynamic simulation of MEA absorption process for CO2 capture from power plants. Int. J. Greenh. Gas Control. 2012;10:295–309. https://doi.org/10.1016/j.ijggc.2012.06.017.

[40] Kvamsdal HM, Jakobsen JP, Hoff KA. Dynamic modeling and simulation of a CO2 absorber column for post-combustion CO2 capture. Chem. Eng. Process. 2009:48(1):135–144. https://doi.org/10.1016/j.cep.2008.03.002.

[41] Hilliard M. A Predictive Thermodynamic Model for an Aqueous Blend of Potassium Carbonate, Piperazine, and Monoethanolamine for Carbon Dioxide Capture from Flue Gas**.** PhD thesis, University of Texas at Austin, 2008.

[42] Kvamsdal H, Rochelle G. Effects of the temperature bulge in CO2 absorption from flue gas by aqueous monoethanolamine. Ind. Eng. Chem. Res. 2008;47(3):867–75. https://doi.org/10.1021/ie061651s.

[43] Poling B, Prausnitz J, O'Connell J. The properties of gases and liquids. New York: McGraw-Hill; 2007.

[44] Weiland RH, Dingman JC, Cronin DJ, Browning GJ. Density and Viscosity of Some Partially Carbonated Aqueous Alkanolamine Solutions and Their Blends. J. Chem. Eng. Data. 1998; 43(3):378–382. https://doi.org/10.1021/je9702044.

[45] Hart W, Watson J, Woodruff D. Pyomo: modeling and solving mathematical programs in Python. Math. Program Comput. 2011;3(3):219–260. https://doi.org/10.1007/s12532-011-0026-8.

[46] Wächter A, Biegler L. On the implementation of an interior-point filter line-search algorithm for large-scale nonlinear programming. Math .Program. 2005;106(1):25–57. https://doi.org/10.1007/s10107-004-0559-y.

[47] Nittaya T, Douglas P, Croiset E, Ricardez-Sandoval L. Dynamic modelling and control of MEA absorption process for CO_2 capture from power plants. Fuel. 2014; 116:672–691. https://doi.org/10.1016/j.fuel.2013.08.031.

[48] Mac Dowell N, Shah N. Identification of the cost-optimal degree of CO_2 capture: An optimisation study using dynamic process models. Int. J. Greenh. Gas Control. 2013;13:44–58. https://doi.org/10.1016/j.ijggc.2012.11.029.

[49] Straathof A, Bampouli A. Potential of commodity chemicals to become bio-based according to maximum yields and petrochemical prices. Biofuels Bioprod. Biorefining. 2017;11(5):798–810. https://doi.org/10.1002/bbb.1786.

[50] Nordhaus W. Revisiting the social cost of carbon. Proc. Nat. Acad. Sci. U.S.A. 2017;114(7): 1518–1523. https://doi.org/10.1073/pnas.1609244114.

[51] Karimi M, Hillestad M, Svendsen H. Capital costs and energy considerations of different alternative stripper configurations for post combustion CO2 capture. Chem. Eng. Res. Des. 2011;89(8):1229–1236. https://doi.org/10.1016/j.cherd.2011.03.005.

[52] Ontario Energy Board. Electricity rates, https://www.oeb.ca/rates-and-your-bill/electricity-rates ; 2021 [accessed 31 August 2021]

[53] Yang B et al. Life cycle environmental impact assessment of fuel mix-based biomass and co-firing plants with CO_2 capture and storage. Appl. Energy. 2019;252:113483. https://doi.org/10.1016/j.apenergy.2019.113483.

[54] Chen W, O'Reilly J, Balance D. Model predictive control of nonlinear systems: Computational burden and stability. IEE. Proc. D. 2000;147(4):387–394. 10.1049/ip-cta:20000379.

[55] Zavala V, Biegler L. The advanced-step NMPC controller: optimality, stability and robustness. Automatica. 2009;45(1):86–93. https://doi.org/10.1016/j.automatica.2008.06.011.

[56] Rúa J, Verheyleweghen A, Jäschke J, Nord LO. Optimal scheduling of flexible thermal power plants with lifetime enhancement under uncertainty. Applied Thermal Engineering. 2021;191:116794. https://doi.org/10.1016/j.applthermaleng.2021.116794.